Experimental Performance Analysis of Salt in Matrix Composites for Thermochemical Heat Storage

Abdullah Ibrahim Al-Ghosini

Submitted to the
Institute of Graduate Studies and Research
in partial fulfillment of the requirements for the degree of

Master of Science
in
Mechanical Engineering

Eastern Mediterranean University
February 2022
Gazimağusa, North Cyprus

Approval of the Institute of Graduate Studies and Research

Prof. Dr. Ali Hakan Ulusoy
Director

I certify that this thesis satisfies all the requirements as a thesis for the degree of Master of Science in Mechanical Engineering.

Prof. Dr. Hasan Hacışevki
Chair, Department of Mechanical Engineering

We certify that we have read this thesis and that in our opinion it is fully adequate in scope and quality as a thesis for the degree of Master of Science in Mechanical Engineering.

Asst. Prof. Dr. Devrim Aydın
Supervisor

Examining Committee

1. Prof. Dr. Fuat Egelioğlu

2. Asst. Prof. Dr. Devrim Aydın

3. Asst. Prof. Dr. Amir Teimourian

ABSTRACT

Thermochemical heat storage (THS) is a promising technology for improving the utilization from renewable energy sources due to its low heat losses, high energy storage density, and long-term heat storage capability. In that regard, synthesis of new sorption materials is critical for advancing THS systems in the future. This study aims to develop composite sorbents and perform energetic, exergetic, and hygro-cyclic analyses for performance comparison of the tested composite sorbents.

In this study, nine different THS materials were synthesized using pumice and vermiculite as the host matrices, and $CaCl_2$, LiCl, $MgCl_2$, $LiNO_3$ as the sorbent salts. The nine sorption materials developed and tested in this study are; P-$CaCl_2$, V-$CaCl_2$, P-LiCl, V-LiCl, P-$MgCl_2$, V-$MgCl_2$, P-$LiNO_3$, V-$LiNO_3$, and P-$CaCl_2$-LiCl. All developed composite materials were tested over four consecutive cycles, and their energetic, exergetic, and hygro-cyclic performances were comparatively investigated. It is worth to mention that the developed pumice-salt composites are novel and have not been investigated previously.

According to the results, the highest energy density of pumice composites was obtained with P-LiCl at 356 kWh/m^3, and the lowest was with P-$LiNO_3$ at 150 kWh/m^3. Similarly, for vermiculite composites, the energy density was obtained highest with V-LiCl at 492 kWh/m^3, and lowest with V-$LiNO_3$ at 205 kWh/m^3. Based on the general observation, the energy density of vermiculite based-salts was higher; however, the desorption capability was lower compared to pumice based-salts. In addition, P-$CaCl_2$-LiCl had the highest energetic cyclic efficiency among pumice

composites (90%), while P-$MgCl_2$ had the lowest with 60%. The highest and lowest energetic efficiencies were found with V-LiCl and V-$LiNO_3$ at 91 and 77%, respectively, for vermiculite composites. The highest exergetic efficiency was obtained with P-LiCl and V-LiCl at 12 and 18%, respectively. The lowest exergetic efficiency were obtained as 3% with P-$MgCl_2$ and 6% with V-$LiNO_3$. According to the testing results, hygro-cyclic efficiencies of pumice-based composites were found higher when compared to vermiculite-based composites. In addition, pumice-based materials showed high structural stability also good thermal performance, and sorption/desorption kinetics over repeating cycles. Whereas vermiculite-based materials showed lower structural stability and desorption capability than pumice composites. The study results showed that the P-$CaCl_2$-LiCl composite provides the highest energetic and hygro-cyclic efficiencies among all the tested sorbents and shows a high exergetic efficiency. Therefore, it could be concluded that pumice based multi-salt composites could be promising THS materials. Further work could be performed in this area for development and optimization of new pumice based multi-salt composites.

Keywords: Thermochemical Heat Storage, Salt in Matrix, Pumice, Vermiculite, Sorption, Desorption, Sorbent, Performance Analysis.

ÖZ

Termokimyasal ısı depolama (THS), düşük ısı kayıpları, yüksek enerji depolama yoğunluğu ve uzun süreli ısı depolama potansiyeli nedeniyle yenilenebilir enerji kaynaklarının kullanımını arttırmak adına önem arz eden bir teknolojidir. Bu bağlamda, THS sistemlerini geliştirmek için sorpsiyon malzemeleri kritik öneme sahiptir. Bu çalışma, kompozit sorbentler üretmeyi, test etmeyi ve test edilen kompozit sorbentleri enerjetik, ekserjetik ve higro-çevrimsel analiz yöntemleriyle karşılaştırmalı olarak incelemeyi amaçlamaktadır.

Bu çalışmada, konukçu matris olarak pomza ve vermikülit ve sorbent tuzları olarak $CaCl_2$, LiCl, $MgCl_2$, $LiNO_3$ kullanılarak dokuz farklı THS malzemesi sentezlenmiştir. Çalışmada geliştirilen ve test edilen dokuz sorpsiyon materyali; P-$CaCl_2$, V-$CaCl_2$, P-LiCl, V-LiCl, P-$MgCl_2$, V-$MgCl_2$, P-$LiNO_3$, V-$LiNO_3$ ve P-$CaCl_2$-LiCl'dir. Geliştirilen tüm kompozit malzemeler dört ardışık çevrimde test edilmiş ve enerjetik, ekserjetik ve higro-çevrimsel performansları karşılaştırmalı olarak incelenmiştir. Çalışma kapsamında geliştirilen tuz-pomza kompozitleri yenilikçi malzemeler olup literatürde daha önce incelenmemişlerdir.

Çalışmada elde edilen sonuçlara göre, pomza kompozitleri için en yüksek enerji yoğunluğu P-LiCl ile 356 kWh/m^3, en düşük enerji yoğunluğu ise P-$LiNO_3$ ile 150 kWh/m^3 olarak elde edilmiştir. Benzer şekilde, vermikülit bazlı kompozitler için, enerji yoğunluğu en yüksek V-LiCl ile 492 kWh/m^3 ve en düşük V-$LiNO_3$ ile 205 kWh/m^3 olarak bulunmuştur. Genel gözleme göre vermikülit bazlı tuzların enerji yoğunluğu pomza bazlı tuzlara göre daha yüksek ancak desorpsiyon kabiliyeti daha

düşük bulunmuştur. Ayrıca, pomza kompozitleri arasında en yüksek ve en düşük çevrimsel enerji verimimine sahip sorbentler sırasıyla 90% ile $CaCl_2$-LiCl ve 60% ile P-$MgCl_2$ olarak belirlenmiştir. Vermikülit bazlı kompozitler için ise en yüksek ve en düşük enerji verimliliği sırasıyla 91% ve 77% ile V-LiCl ve V-$LiNO_3$ kullanılan testlerde elde edilmiştir. En yüksek ekserji verimine sahip kompozitler sırasıyla 12% ve 18% ile P-LiCl ve V-LiCl olarak bulunmuştur. En düşük ekserjetik verim ise, 3% ile P-$MgCl_2$ ve 6% ile V-$LiNO_3$ kullanıldığı duruma elde edilmiştir. Test sonuçlarına göre, pomza esaslı kompozitlerin higro-çevrimsel verimleri, vermikülit esaslı kompozitlere göre daha yüksek bulunmuştur. Ek olarak, pomza bazlı malzemeler yüksek yapısal ve çevrimsel stabilite, ayrıca etkin ısıl performans ve sorpsiyon/desorpsiyon kinetiği göstermiştir. Vermikülit esaslı malzemelerin ise, pomza kompozitlerine göre daha düşük yapısal stabilite ve desorpsiyon kabiliyetine sahip olduğu görülmüştür. Çalışma sonuçları, P-$CaCl_2$-LiCl kompozitinin, test edilen tüm sorbentler arasında en yüksek enerjik ve higro-çevrimsel verimliliğe sahip olduğunu ayrıca ekserji veriminin de etkin bir değerde olduğunu göstermiştir. Bu nedenle, pomza esaslı tuz karışımlı kompozitlerin yüksek performanslı sorbentler geliştirme yönünde etkin bir yöntem olduğu sonucuna ulaşılmıştır. Bu sebeple bu tür malzmelerin geliştirilmesi ve optimize edilmesi için ileri çalışmalar yapılması faydalı olacaktır.

Anahtar Kelimeler: Termokimyasal Isı Depolama, Tuz Emdirilmiş Matris, Pomza, Vermikülit, Sorpsiyon, Desorpsiyon, Sorbent, Performans Analizi.

ACKNOWLEDGMENT

I would like to thank my parents and sister for their support and motivation throughout my thesis and general academic career. Thank you very much for your words of encouragement, and I will be grateful and strive to make you proud. I would also like to thank all of my family and best friends for their motivation and support.

I would also like to thank my thesis supervisor Assist. Prof. Dr. Devrim Aydin for his unlimited support and guidance throughout this thesis's real progress. With the experience and innovative ideas of Dr. Devrim helped me a lot to improve the research. Thank you very much, and I will be happy to work with you again.

This thesis was supported by TUBITAK's project numbered 119M073, and I would like to thank the Scientific and Technological Research Council of Turkey (TUBITAK) for their support.

TABLE OF CONTENTS

LIST OF TABLES

LIST OF FIGURES

LIST OF SYMBOLS AND ABBREVIATIONS

a	Air
AAO	Anodic Aluminum Oxide
A/C	Air Conditioning
ads	Adsorbent
avg	Average
ch	Charging
cum	Cumulative
C_p [J/kg.K]	Specific Heat at Constant Pressure
d	Dry
dch	Discharging
dsorp	Desorption
E_{cum} [kWh]	Cumulative Thermal Energy
$\dot{E}x$ [kW]	Exergy rate
Ex_{cum} [kWh]	Cumulative Thermal Exergy
E_d [kWh/m^3]	Energy Density
$\dot{f}_{sorp}$ [kJ/g]	Sorption Rate
$\dot{f}_{dsorp}$ [kJ/g]	Desorption Rate
H [kJ/s]	Enthalpy
in	Inlet
LHS	Latent Heat Storage
m [kg]	Mass
$\dot{m}$ [kg/s]	Mass Flow Rate

max	Maximum
MOF	Metal-organic Framework
out	Outlet
P	Pumice
$\dot{Q}$ [kW]	Heat Flow Rate
RH [%]	Relative Humidity
S [kJ/s]	Entropy
SHS	Sensible Heat Storage
SIM	Salt In Matrix
sorp	Sorption
t [s]	Time
T [°C]	Temperature
TES	Thermal Energy Storage
THS	Thermochemical Heat Storage
v [m/s]	Velocity
V	Vermiculite
V [m^3]	Volume
w [g/kg]	Absolute Humidity
y	Mass Uptake/loss Ratio
Z	Zeolite
Δ	Difference
ρ [kg/m^3]	Density
η_I [%]	1st law Efficiency
η_{II} [%]	2nd law Efficiency
$\eta\eta_{hyg}$ [%]	Hygro-Cyclic Efficiency

Chapter 1

INTRODUCTION

1.1 Background

Recently, thermal energy has shown a significant increase in demand due to increasing population and comfort standards. Thermal energy storage (TES) systems play an important role in increasing the utility of renewable energy sources, therefore reducing the reliance on fossil fuels [1], [2]. Thermochemical heat storage (THS) systems have high energy density and low heat loss during the storage phase compared with latent heat storage (LHS) systems and sensible heat storage (SHS) systems [3]. Therefore, THS systems are considered as a good alternative for thermal energy storage. To the best of the author's knowledge, such systems are not extensively studied compared to other TES systems, and not available in the commercial market, and are currently in the research and development phase. THS systems operate based on reversible absorption and desorption over discharging and charging cycles respectively.

The potential sources that can be used for charging the THS material are solar thermal collectors, industrial waste heat, off-peak electricity, photovoltaic panels, and etc. The material used in THS systems can be charged using any renewable sources (i.e., solar air heater) in summer and then discharged to heat the spaces at any time in winter. It can be discharged at the peak hours of electricity consumption to reduce the peak load on the electricity grid [4]. In addition, off-peak electricity or photovoltaic panels can be used to charge the sorbent by supplying heat using electric heaters and discharging

it at another time. The THS sorption material could be used as seasonal storage, where it can store the heat for a long-term (i.e., 3-6 months) from summer to winter or short-term (i.e., 3-4 days) [3].

There are different materials used for the three TES systems. The most common materials used in SHS are water, brick, soil, and rock, and the SHS system is usually applied in large plants. LHS used salts, ice, and paraffin as materials and is commonly used in low heat temperature sources [5]. For THS system, the most commonly developed materials are Silica and Zeolite, but recently more investigations and developments were carried out on new different materials. Most commonly investigated salts in the last decade are $CaCl_2$, the highest hygroscopic salts recently commonly used are $CaCl_2$, LiCl, $MgCl_2$, and $LiNO_3$.

The THS reactor can be designed either as open or closed system. Open systems are designed as a reactor open to the surrounding environment and worked at atmospheric pressure. Closed systems are designed as reactors insulated from the surroundings and operate below atmospheric pressure. In addition, the open THS systems usually used air as a process fluid, whereas closed systems use water as a process fluid [6]. Different parameters can influence the efficiency of the THS system. For example, material type and size, airflow rate, amount of moisture, and level of heat used to charge the materials affect the system's performance.

1.2 Thesis Aim and Objectives

This experimental study aims to develop, test and investigate nine different sorption materials for the THS system for space heating and demonstrate the importance of THS materials/systems for enhancing the use of renewables.

The objectives of this experimental study;

- To develop, test and investigate nine different sorption materials of P-$CaCl_2$, V-$CaCl_2$, P-LiCl, V-LiCl, P-$MgCl_2$, V-$MgCl_2$, P-$LiNO_3$, V-$LiNO_3$, and P-$CaCl_2$-LiCl as alternatives to the conventional THS materials (i.e., Silica gel, Zeolite).
- To evaluate the cyclic performance of the nine sorbents over discharging/charging cycles within the developed prototype open THS unit.
- To investigate which materials are most suitable for solar-driven THS applications.

1.3 Novelty of the Research

Open THS system is a relatively a new method, and only limited amount of research is performed on it. In the literature, Zeolite, Silica gel, activated carbon, and several different composites (i.e., salt impregnated vermiculite) are widely investigated as candidate sorption materials. However, there is no study investigating the performance of different salt impregnated composite sorbents using pumice as the host matrix. Accordingly, in this research, four new inorganic salts (i.e., $CaCl_2$, LiCl, $MgCl_2$, and $LiNO_3$) and one mixture of two inorganic salts (i.e., $CaCl_2$-LiCl) are impregnated into two host matrices of pumice and vermiculite. Overall, in this research, nine different sorbents of P-$CaCl_2$, V-$CaCl_2$, P-LiCl, V-LiCl, P-$MgCl_2$, V-$MgCl_2$, P-$LiNO_3$, V-$LiNO_3$, and P-$CaCl_2$-LiCl have been investigated and experimentally analyzed.

1.4 Thesis Structure

The structure of the presented study consists of the following:

Chapter 1: Gives a background on THS systems, aims and objectives, and the novelty of this experimental study.

Chapter 2: Presents the literature review regarding the THS systems and materials and their operating principles. Finally, the recent studies of the THS materials were summarized.

Chapter 3: Shows the design and operations of the THS system. In addition, the thermodynamics analysis of the open THS system investigated in this study was presented.

Chapter 4: Shows the material selection, synthesis, and testing rig used during the experiment. In addition, the experimental setup and methodology of the THS system were presented.

Chapter 5: Presents the experimental results and discussions of discharging, charging, and overall performance analysis. In addition, energy, exergy, and moisture sorption/desorption analysis were calculated.

Chapter 6: Summarizes the conclusion of the outcomes obtained from this work. Additionally, the future work of this research was explained.

Chapter 2

LITERATURE REVIEW

2.1 Background and Review of State of the Art of THS Materials

Many researchers have recently focused on new sorption materials, and several different investigations were performed in that area. The following characteristics are used to determine an appropriate sorption material for the THS system: i) higher energy density, ii) higher rate of sorption/desorption, iii) high rate of mass and heat transfer, iv) lower cost of energy produced, v) environmentally-friendly (non-toxic).

As discussed in Gaeini et al. [7], many methods were used to stabilize different sorption materials using host matrix such as vermiculite, ethyl cellulose, and expanded graphite, with inorganic salts such as $CaCl_2$.The kinetics and energy density of the materials are shown based on the stabilization techniques on material performance. Among the three composite materials investigated, the energy density of the twice-impregnated inorganic salt ($CaCl_2$) into the host matrix (vermiculite) was determined as the highest with around 1.2 GJ/m^3.

Nejhad et al. investigated composite sorbents of P-$CaCl_2$, V-$CaCl_2$, and Zeolite. The developed composite P-$CaCl_2$ is novel, and no previous studies show its performance in THS. The experimental analysis of the open system was done with three cycles of discharging/charging to test the stability of the sorption materials [8]. Five hours of discharging and two hours of charging were adjusted during the experiment. In

addition, the inlet temperature of charging was around (T_{ch} = 85 – 95 °C). As a result of the tests, the energy densities of the sorbent materials of P-$CaCl_2$, V-$CaCl_2$, and Zeolite were obtained as 187, 174, and 183 kWh/m^3, respectively. The energetic efficiencies of P-$CaCl_2$, V-$CaCl_2$, and Zeolite were found in the range of 77-75 %, 72-70 %, and 61-58 %, respectively. The exergetic efficiencies were calculated in the range of 5.3-5.2 % for P-$CaCl_2$, 9.1-7.4 % for V-$CaCl_2$, and 20.5-8.3 % for Zeolite. Moreover, the hygrothermal efficiencies of P-$CaCl_2$, V-$CaCl_2$, and Zeolite were obtained in the range of 89.5-77.4 %, 84.8- 75.2 %, and 32.6-35.3 %.

In 2021, Zhang et al. [9] constructed a demonstrative prototype and prepared a composite material of $SrCl_2$. The working pair of $SrCl_2$-NH_3 was investigated as the longest duration of heat storage for THS. Under the conditions of discharging temperature of 40 °C, charging temperature of 92 °C, and evaporation temperature of -5 °C, the energy storage density was determined to be about (1630 kJ/kg $SrCl_2$) or (1386 kJ/kg composite sorbent). Therefore, when the discharging temperature increases, the heat storage efficiency of the THS decreases. In contrast, the coefficient of performance increased when the discharging temperature increased. The sorption material's heat storage efficiency and coefficient of performance were obtained as 68.7 % and 40.5 %, respectively. The experimental results showed that the THS is efficient for long-duration heat storage applications. In the charging phase, the industrial waste heat recovery and solar air heater can be used to charge the material during summertime.

Jarimi et al. [3], investigated which sorption materials are suitable for building heat storage applications powered by solar energy in both the long-term and short-term. The study shows a difference of individual and mixture salts impregnated into

vermiculite. LiCl, $CaCl_2$, $MgCl_2$, and $MgSO_4$ were chosen in the study since these salts are highly hygroscopic compared to others. For the mixture of composite salts, the energy density of V-$MgSO_4$-$CaCl_2$, V-$CaCl_2$-LiCl, and V-$MgSO_4$-$MgCl_2$ was founded as 1752, 1293, and 1030 kJ/kg, respectively. In addition, the energy densities of the individual composite salts of LiCl, $CaCl_2$, $MgCl_2$, and $MgSO_4$ were determined as 1147, 870, 696, and 1014 kJ/kg, respectively. The study proved that the vermiculite with salts mixture is more suitable for THS applications since the energy densities are generally 250 kJ/kg higher than individual salts. Moreover, it is determined that increasing the ratio of $CaCl_2$ in the mixtures will improve the rate of sorption and amount of moisture uptake.

Aydin et al. experimentally investigated the overall performance of the composite salt of $CaCl_2$ impregnated into vermiculite in their open-sorption pipe reactor for THS systems [10]. Several parameters were obtained during the experiment. Finding absolute humidity difference (Δw) is used for determining the critical moisture level for each material. The critical moisture level of the V-$CaCl_2$ was obtained around 11.2 g/kg. In the four testing cycles, the sorbent material delivers a significant temperature rise during the discharge phase. The volume of the sorption material was 0.088 m^3, in which the sorbent material provides cumulative energy of 25.5 kWh and energy density of 290 kWh/m^3. Additionally, the energetic and exergetic efficiencies were found in the range of 69-64 % and 21-14 %, respectively.

In 2018, Aydin et al. developed and investigated an integrated heat pump thermal system and sorbent [11]. The system can convert the excess electricity to store the heat in the sorption material for later use. Five different materials were tested in the prototype system. With a volume of 0.04 m^3 of a sorbate, the cumulative energy

produced during 1200 min of discharging time was 6.8 kWh. Additionally, with the use of V-$CaCl_2$, the energy density was obtained as 170 kWh/m^3 and the COP was calculated as 2.39. The results were found similarly in both experiment and numerical simulation.

Casey et al. [12] analyzed the performance of sorbents materials through large-scale experiments. Many parameters were obtained from the experimental test, such as energy, exergy, and hydrothermal efficiency. Zeolite provides the highest desorption rate in the charging phase, and it has a fast kinetic reaction. For open THS, the V-$CaCl_2$ was found that it is the most promising candidate compared to others Salt In Matrix (SIM), since it produces a high amount of heat and it can absorb a high amount of vapor in discharging phase. The energy density of the V-$CaCl_2$ in 1^{st} cycle was calculated as 160 kWh/$m^{3,}$ and it was the highest compared to others SIM. In 4^{th} cycle, the energy density was found as 120 kWh/$m^{3,}$ and it was also was highest against others. The decrease in the energy density during the cycles was because of insufficient time of heating temperature (T_{ch} = 90 °C) to remove all absorbed moisture from the sorption material during the charging phase. The energy and exergy efficiencies in the four cycles of the SIM were found in the range of 63-65 % and 6-4 %, respectively. Additionally, V-$CaCl_2$ generates lower heat than Zeolite, but it is considered to generate high heat with the lowest up-taking vapor. Moreover, V-$CaCl_2$ is steadier in terms of hygrothermal cyclic behavior.

Zondag et al. studied the sorption material ($MgCl_2$. 6H2O) for the THS system [13]. The concept of the system was an open THS prototype. The packed bed of the sorption material was 0.017 m^3 (17 L) and generating heat of 0.15 kW. Moreover, the energy density of the system was calculated as 0.5 $GJ/m^3$with an instantaneous COP of 12.

In 2019, Shere et al. presented a study on THS sorption materials [14]. The sorbate is composed of a mixture of inorganic salts ($MgCl_2$, $MgSO_4$), and the (graphite, carbon) were impregnated into the host matrix of Zeolite 13X. Simultaneous thermal analysis (STA) was used to analyze energy storage and adsorption/desorption rates by combining differential scanning calorimetry (DSC) and thermogravimetric (TG). With a range of temperature between 30-150 ℃, the energy density of the sorbate was obtained as 400 kJ/kg. Additionally, the sorbent's thermal characteristics leads it to be a good choice for thermal storage in buildings.

In 2020, Yilmaz et al. investigated a new anodization method of an anodic aluminum oxide (AAO) which is used as a host matrix for the THS system [15]. Four hygroscopic salts ($CaCl_2$, $MgCl_2$, LiCl, and $LiNO_3$) were tested as individual salts impregnated in the AAO templates, and four mixtures of hygroscopic salts were also tested. The morphology of the AAO composites was examined using electron microscopy. From the individual inorganic salts, the energy densities of the LiCl, $LiNO_3$, $MgCl_2$, and $CaCl_2$ were found as 242, 251,231, and 220 kJ/kg, respectively, where $LiNO_3$ has the highest energy density compared to other individual salts. In addition, the energy densities for the mixture composites salts of $CaCl_2$+LiCl (1:1), LiCl+ $LiNO_3$ (1:1), $CaCl_2$+ $LiNO_3$ (1:1), and LiCl+ $LiNO_3$ (1:3) were found as 327, 468, 168, and 199, respectively. From the results of the energy densities of salts mixture composites, the LiCl+ $LiNO_3$ (1:1) generates much higher than others mixtures.

Several different inorganic salts such as ($CaCl_2$, LiCl, $MgCl_2$, $MgSO_4$, $LiNO_3$, $SrCl_2$, others.) and natural sorbents (Silica Gel, Zeolite) have been extensively researched and tested for THS. At present, only a small number of host matrices (i.e., Wakkanai siliceous shale, vermiculite, activated carbon, and activated alumina) have been

examined for salt impregnation. From previous studies, it is shown that there is a gap in terms of impregnated salts in new porous host matrices. Previously in several researches (Nejhad et al. [8], Jarimi et al. [3], Aydin et al. [10], [11], and Casey et al. [12]), V-$CaCl_2$ (Salt-In-Matrix) was tested and found that it is an efficient sorption material for open THS system. In 2019, a new composite of pumice and $CaCl_2$ was developed and experimentally analyzed by Nejhad et al. [8], and it is found that using pumice as a host matrix it keeps the composite material structurally stable while repeating many cycles. In contrast, vermiculite shows disadvantages in terms of stability, where it is physically degradation due to the high absorption of moisture during repeating cycles.

In the current study, new novel hygroscopic salts with pumice are tested and compared with salt impregnated vermiculate composites. Accordingly, new four inorganic salts (i.e., $CaCl_2$, LiCl, $MgCl_2$, and $LiNO_3$) and a mixture of two inorganic salts (i.e., $CaCl_2$-LiCl) are impregnated into two host matrices of pumice and vermiculite. Overall, nine different sorbents of P-$CaCl_2$, V-$CaCl_2$, P-LiCl, V-LiCl, P-$MgCl_2$, V-$MgCl_2$, P-$LiNO_3$, V-$LiNO_3$, and P-$CaCl_2$-LiCl have been developed and experimentally analyzed in this study.

From Table 1, we can see the summary of the previous studies on thermochemical materials. Heat energy densities, energetic and exergetic efficiencies are presented in Table 1.

Table 1: Overall Summary of Previous Studies of Sorption Materials.

	Material	No. of cycles	Heat energy density	η_I (%)	η_{II} (%)
Nejhad et al. [8]	P-$CaCl_2$	3	196-175 kWh/m^3	77-75	5.3-5.2
	V-$CaCl_2$	3	181-164 kWh/m^3	72-70	9.1-7.4
	Zeolite	3	250-115 kWh/m^3	61-58	20-8.3
Zhang et al. [9]	$SrCl_2$	1	1630 kJ/kg	-	-
Jarimi et al. [3]	V-LiCl	1	1147 kJ/kg	-	-
	V-$CaCl_2$	1	870 kJ/kg	-	-
	V-$MgCl_2$	1	696 kJ/kg	-	-
	V-$MgSO_4$	1	1014 kJ/kg	-	-
Aydin et al. [10]	V-$CaCl_2$	4	290 kWh/m^3	69-64	21-14
Aydin et al. [11]	V-$CaCl_2$	1	170 kWh/m^3	-	-
Casey et al. [12]	V-$CaCl_2$	4	160-120 kWh/m^3	63-65	6-4
	Zeolite	4	114-56 kWh/m^3	89-82	23-5
	Silica Gel	4	44-40 kWh/m^3	64-63	10-4
Zondag et al. [13]	$MgCl_2$-6H2O	1	0.5 GJ/m^3	-	-
Shere et al. [14]	Z-$MgCl_2$-$MgSO_4$	1	400 kJ/kg	-	-
Yilmaz et al. [15]	AAO-LiCl	1	242 kJ/kg	-	-
	AAO-$LiNO_3$	1	251 kJ/kg	-	-
	AAO-$MgCl_2$	1	231 kJ/kg	-	-
	AAO-$CaCl_2$	1	220 kJ/kg	-	-
Courbon et al. [16]	Silica gel-$CaCl_2$	1	211 kWh/m^3	-	-
Van Alebeek et al. [17]	Zeolite 13X	1	136 kWh/m^3	-	-
Haije et al. [18]	LiCl–$MgCl_2$	1	222 W/kg	-	-
Xueling et al. [19]	Zeolite 13X-$CaCl_2$-$MgSO_4$	1	1414 J/g	-	-
Courbon et al. [20]	Silica gel-$SrBr_2$	1	203 kWh/m^3	-	-
Yu et al. [21]	Silica gel-LiCl	1	163 kWh/m^3	-	-
Grekova et al. [22]	V-LiCl	1	253 kWh/m^3	-	-
Yan et al. [22]	Expanded graphite-$MnCl_2$-NH_3	1	179 kWh/m^3	-	-
Ans et al. [23]	MOF-$SrBr_2$	1	233 kWh/m^3	-	-
Xu et al. [24]	Zeolite 13X-$MgSO_4$	1	123 kWh/m^3	-	-
Piperopoulos et al. [25]	Exfoliated graphite-$Mg(OH)_2$	1	1250 kJ/kg	-	-
Shi et al. [26]	MOF-SO_3H-$CaCl_2$	1	1274 J/g	-	-
Courbon et al. [27]	Silica gel-LiBr	1	246 kWh/m^3	-	-
Zhang et al. [28]	Activ. alumina-LiCl	1	191 kWh/m^3	-	-

Chapter 3

DESIGN AND THERMAL ANALYSIS OF THS SYSTEM

3.1 System Design and Operation

Recently, thermal energy storage systems have become more needful and essential, especially with solar applications. Sensible heat storage (SHS) and latent heat storage systems (LHS) are the available thermal energy storage systems. Still, these systems suffer from low energy storage and density, and fluctuations in temperature and drops. As a result, a new approach of THS is presented in this work as heat storage with reversible absorption and desorption processes, as illustrated in Figure 1.

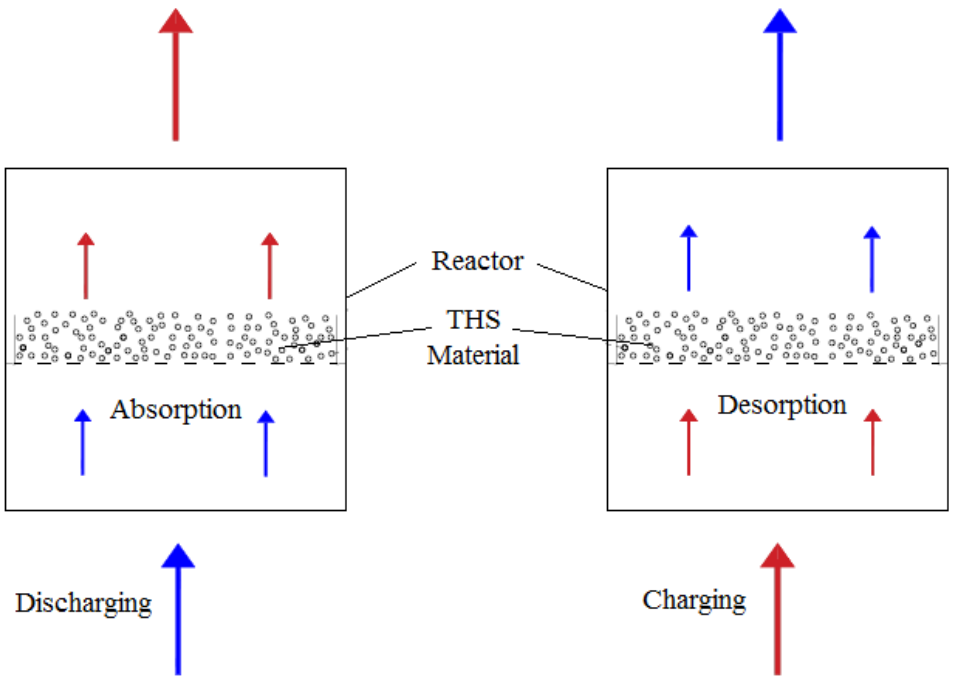

Figure 1: Basic Principles of Open Sorption Reactor System.

Inadequate heat transmission and irregular airflow can severely decline the THS prototype performance, so the design of the THS system is essential to increase the storage efficiency of the sorbents. Therefore, the design of the system appears to be one of the most critical criteria for the reactor's operating stages. A good THS should have a constant discharge temperature, a consistent moisture sorption rate, and efficient heat transmission with minimum heat losses.

3.1.1 Design of THS Prototype

The developed THS testing unit (see Figure 2) consists of two parts; the A/C unit and THS reactor. The A/C unit consists of a radial fan, ultrasonic humidifier (used only in discharging process), and electric heater coils (used only in the charging process). THS reactor is designed as a rectangular-shaped box (370 × 330 × 460 mm) covered with an insulation of 40 mm foil-lined glass wool, and internally it has a rectangular wire mesh tray (350 × 310 × 32 mm) that is placed horizontally in the middle of the reactor. The reactor was insulated to prevent heat losses to the external environment. The sorption material is held in a wire mesh tray and perpendicular to the airflow. A radial fan controls the prototype's air flow rate. The air-conditioning system regulates the temperature of the experimental environment. The air is heated by four electric heaters; two are 1 kW, and the other two are 0.5 kW and controlled by sensors. The amount of moisture in the system is increased by the humidifier. Sensors are used to measure and record the relative humidity and ambient, inlet, outlet temperatures during discharging and charging operations.

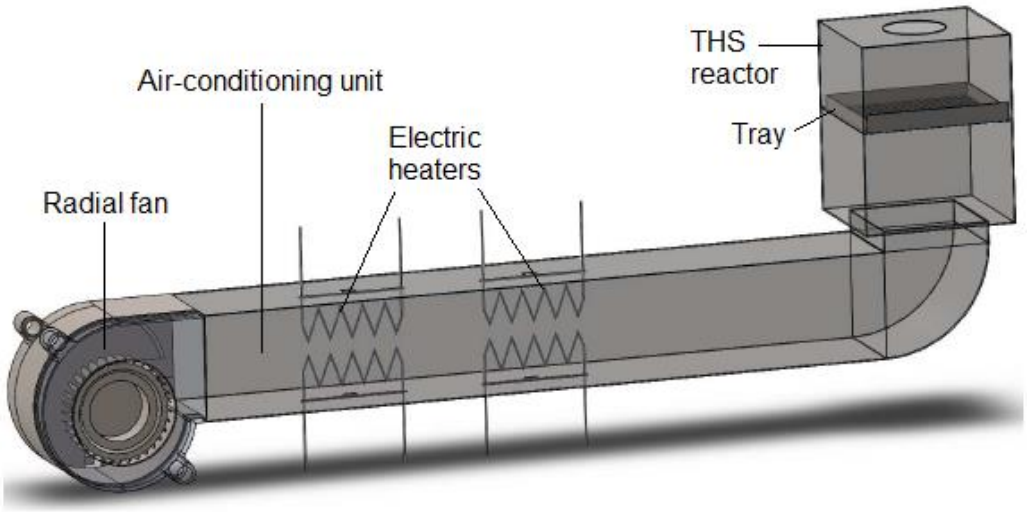

Figure 2: 3D View of the Designed THS System.

3.1.2 System Operation Description

The schematic illustration of the discharging and charging processes of the developed experimental unit is given in Figure 3. In the open system, the ambient air is humidified up to 80 – 85 % of relative humidity during the discharging process using an ultrasonic humidifier. The radial fan blows humidified air through the rectangular duct to the THS reactor. At the reactor inlet, the air temperature was around 19 to 23 °C. When the moist air reaches the sorption bed and passes across the sorption material, the sorption material absorbs the moisture, and as a result, heat is generated. The low moisture content hot air is expelled from the system at the end of the procedure. In the charging phase, the electric coils heat the air to 80 – 85 °C. Then, the fan blows the heated air to the sorption bed. The moisture is removed from the sorption material, and the moist air is expelled from the system.

The weight of the sorbent was measured after every discharging and charging process during the experiment to determine the amount of moisture absorbed and adsorbed in discharging and charging cycles, respectively. From the results of the weights, sorption and desorption rates are obtained. The overall summary of the operation procedure of

discharging and charging processes during the experimental testing is shown in Figure 4.

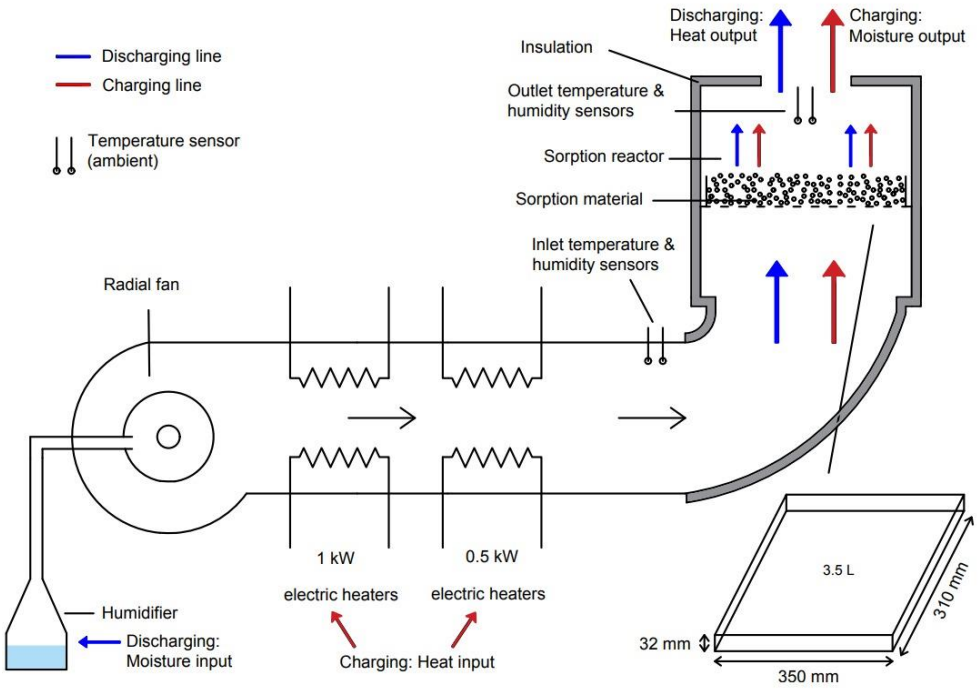

Figure 3: Schematic Illustration of the Open THS System with Discharging and Charging Operations.

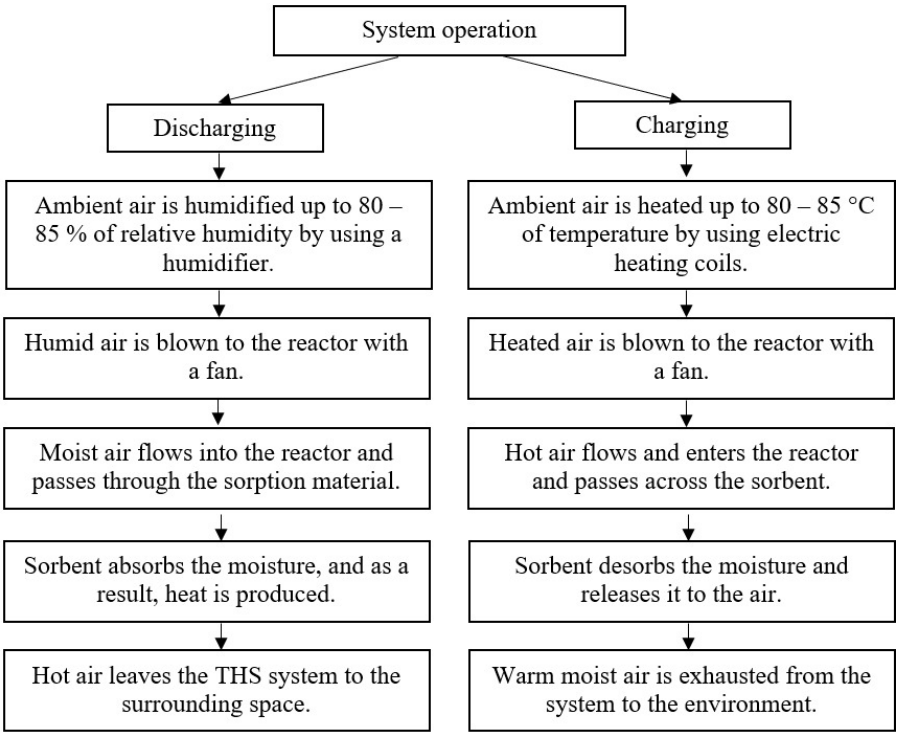

Figure 4: System Operation Procedure of Discharging and Charging Processes.

3.2 Thermodynamic Analysis of the Open THS System

In order to show the performance of the nine different sorbent materials of THS system, energetic and exergetic efficiencies will be examined based on the first law and second law of thermodynamics. Exergy is the amount of useful potential work that can be used from the system [29]. Several thermodynamic factors are calculated from the parameters obtained during the experiment by the sensors, such as energy ($\dot{Q}, E$), exergy ($\dot{E}x$), first law efficiency (η_I), second law efficiency (η_{II}), hygro-cyclic efficiency (η_{hyg}), sorption and desorption rate ($\dot{f}$), energy density (E_d) and mass uptake/loss ratio (y).

3.2.1 Exergy and Energy Analysis of the System

The heat output rate ($\dot{Q}_{out}$) is determined based on the enthalpy changes before and after the sorption material.

$$\dot{Q}_{out} = \dot{H}_{out} - \dot{H}_{in} \tag{1a}$$

$$\dot{Q}_{out} = \dot{m}_{dch} C_p (T_{out} - T_{in}) \tag{1b}$$

Where $\dot{H}_{out}$ is enthalpy output rate, $\dot{H}_{in}$ is enthalpy input rate, $\dot{m}_{dch}$ is discharging mass flow rate, and C_p is specific heat at constant pressure.

The cumulative energy output and input ($E_{out,dch,cum}$, $E_{in,ch,cum}$) of discharging and charging phases are calculated by time integration of Eq. (1b). The cumulative energy output and input equations are shown below;

$$E_{out,dch,cum} = \dot{m}_{dch} C_p \int_0^{t_{dch}} (T_{out} - T_{in}) dt \tag{2}$$

$$E_{in,ch,cum} = \dot{m}_{ch} C_p \int_0^{t_{ch}} (T_{in} - T_{out}) dt \tag{3}$$

Where t_{dch} is discharging time, T_{out} is temperature output, T_{in} is temperature input, $\dot{m}_{ch}$ is charging mass flow rate, and t_{ch} is charging time.

Instantaneous exergy output rate ($\dot{E}x_{out,dch}$) for discharging and charging processes are obtained based on the exergetic variations before and after the reactor (Eq. (4a)).

$$\dot{E}x_{out,dch} = (\dot{E}x_{out} - \dot{E}x_{in}) \tag{4a}$$

Where $\dot{E}x_{out}$ is exergy output rate, and $\dot{E}x_{in}$ is exergy input rate.

The exergy output can be defined as the difference of air enthalpy and entropy across the reactor (Eq. (4b)). In addition, the temperature in exergy analysis is calculated in Kelvin unit.

$$\dot{E}x_{out,dch} = \dot{m}_{dch}[(h_{out} - h_{in}) - T_a(s_{out} - s_{in})] \tag{4b}$$

Where h_{out} is enthalpy output, h_{in} is enthalpy input, s_{out} is entropy output, and s_{in} is entropy input.

The exergy output and input are expressed by Eqs. (4c) and (5);

$$\dot{E}x_{out,dch} = \dot{m}_{dch}C_p\left[(T_{out} - T_{in}) - T_a \ln\left(\frac{T_{out}}{T_{in}}\right)\right] \tag{4c}$$

$$\dot{E}x_{in,ch} = \dot{m}_{ch}C_p\left[(T_{in} - T_{out}) - T_a \ln\left(\frac{T_{in}}{T_{out}}\right)\right] \tag{5}$$

Where T_a is the ambient temperature.

The cumulative exergy output and input ($Ex_{out,dch,cum}$, $Ex_{in,ch,cum}$) for discharging and charging phases, which are calculated by time integration of Eqs. (4c) and (5) as shown below:

$$\mathrm{Ex_{out,dch,cum}} = \dot{\mathrm{m}}_{\mathrm{dch}}\mathrm{C_p}\int_0^{t_{dch}}\left[(\mathrm{T_{out}}-\mathrm{T_{in}})-\mathrm{T_a}\ln\left(\frac{\mathrm{T_{out}}}{\mathrm{T_{in}}}\right)\right] \quad (6)$$

$$\mathrm{Ex_{in,ch,cum}} = \dot{\mathrm{m}}_{\mathrm{ch}}\mathrm{C_p}\int_0^{t_{ch}}\left[(\mathrm{T_{in}}-\mathrm{T_{out}})-\mathrm{T_a}\ln\left(\frac{\mathrm{T_{in}}}{\mathrm{T_{out}}}\right)\right] \quad (7)$$

The energetic efficiency (η_{I}) (first law efficiency) of THS is expressed by Eq. (8).

$$\eta_{\mathrm{I}} = \frac{\mathrm{E_{out,dch,cum}}}{\mathrm{E_{in,ch,cum}}} \quad (8)$$

The exergetic efficiency (η_{II}) (second law efficiency) of THS is obtained by Eq. (9).

$$\eta_{\mathrm{II}} = \frac{\mathrm{Ex_{out,dch,cum}}}{\mathrm{Ex_{in,ch,cum}}} \quad (9)$$

The hygro-cyclic efficiency (η_{hyg}) of THS material is obtained by Eq. (10).

$$\eta_{\mathrm{hyg}} = \frac{m_{dch,f}-m_{ch,f}}{m_{dch,f}-m_{dry}} \quad (10)$$

Where $m_{dch,f}$ is final mass of discharging, $m_{ch,f}$ is final mass of charging, and m_{dry} is dry mass.

The absolute humidity (w) based on the relative humidity and temperature of air is determined by Eq. (11);

$$w = 216.7\left[\frac{\frac{\emptyset}{100\%}6.112\exp\left(\frac{17.62\mathrm{T}}{243.12+\mathrm{T}}\right)}{273.15+\mathrm{T}}\right] \quad (11)$$

The partial pressure of vapor of air is obtained by;

$$\mathrm{P_w} = \frac{\emptyset\mathrm{P_{w,sat}}}{100\%} \quad (12)$$

Where $\mathrm{P_w}$ is water vapor partial pressure, $\emptyset$ is relative humidity, and $\mathrm{P_{w,sat}}$ is water vapor saturation pressure.

The sorption rate ($\dot{f}_{sorp}$) of moisture from the sorbent material in discharging phase can be calculated at any time during the process (Eq. (13)). Similarly, desorption rate ($\dot{f}_{dsorp}$) of moisture in the charging phase can be obtained from Eq. (14);

$$\dot{f}_{sorp} = \int_{t_{x,dch}}^{t_{x+1,dch}} \dot{m}_{dch} C_p \, (w_{in} - w_{out}) dt \tag{13}$$

$$\dot{f}_{dsorp} = \int_{t_{x,ch}}^{t_{x+1,ch}} \dot{m}_{ch} C_p \, (w_{out} - w_{in}) dt \tag{14}$$

Where w_{in} is inlet absolute humidity, and w_{out} is outlet absolute humidity.

The mass changes (Δm) of the sorbent are calculated by taking the difference of the dry and wet weights (m_{dry}, m_{wet}) (Eq. (15));

$$\Delta m = m_{wet} - m_{dry} \tag{15}$$

Eqs. (16) and (17) are used to calculate the mass taken (Δm_{dch}) and losses (Δm_{ch}) of moisture from the sorbent.

$$\Delta m_{dch} = \int_{0}^{t_{dch}} \dot{m}_{dch} C_p \, (w_{in} - w_{out}) dt \tag{16}$$

$$\Delta m_{ch} = \int_{0}^{t_{ch}} \dot{m}_{ch} C_p \, (w_{out} - w_{in}) dt \tag{17}$$

The total mass uptake ratio of discharging phase (y_{dch}) is the total desorbed sorbate per the mass of dry adsorbent ($m_{ads,dry}$) (Eq. (18)). In addition, the total mass loss ratio of the charging phase (y_{ch}) is the total desorbed sorbate per the mass of wet adsorbent ($m_{ads,wet}$) (Eq. (19));

$$y_{dch} = \left[\int_{0}^{t_{dch}} \dot{m}_{dch} C_p \, (w_{in} - w_{out}) dt \right] / m_{ads,dry} \tag{18}$$

$$y_{ch} = \left[\int_0^{t_{ch}} \dot{m}_{ch} C_p \, (w_{out} - w_{in}) dt\right] / m_{ads,wet} \quad (19)$$

Based on the calculated factor $E_{out,dch,cum}$ (Eq. (2)), we can obtain the energy density of the sorbent material. The energy density is the storage performance of the sorbent material during the discharging process (Eqs. (20) and (21));

$$E_d = \frac{E_{out,dch,cum}}{V_{ads}} \quad (20)$$

$$E_d = \frac{E_{out,dch,cum}}{\Delta m_{dch}} \quad (21)$$

Where E_d is the energy density, and V_{ads} is adsorbent volume.

3.3 Uncertainty Analysis

The uncertainty analysis is a technique used to calculate the error/accuracy percentages of the experimental results. Based on Gauss propagation law, the uncertainties were determined for this experiment. The uncertainty of distinct, independent variables (w_R) is represented by the w_1, w_2, w_3, …, w_n variables [30].

$$w_R = \left[\left(\frac{\partial R}{\partial x_1} w_1\right)^2 + \left(\frac{\partial R}{\partial x_2} w_2\right)^2 + \left(\frac{\partial R}{\partial x_3} w_3\right)^2 + \cdots + \left(\frac{\partial R}{\partial x_n} w_n\right)^2\right]^{1/2} \quad (22)$$

To find the total uncertainty of any parameter, for example, η_I is a function of $T_{out,dch}$, $T_{in,dch}$, $T_{out,ch}$, $T_{in,ch}$, m_{dch}, and m_{ch}, so they can be calculated as;

$$w_{\eta_I} = \left[\left(\frac{\partial \eta_I}{\partial T_{out,dch}} w_{T_{out,dch}}\right)^2 + \left(\frac{\partial \eta_I}{\partial T_{in,dch}} w_{T_{in,dch}}\right)^2 + \left(\frac{\partial \eta_I}{\partial T_{out,ch}} w_{T_{out,ch}}\right)^2 + \left(\frac{\partial \eta_I}{\partial T_{in,ch}} w_{T_{in,ch}}\right)^2 + \left(\frac{\partial \eta_I}{\partial m_{dch}} w_{T_{in,ch}}\right)^2 + \left(\frac{\partial \eta_I}{\partial m_{ch}} w_{m_{ch}}\right)^2\right]^{1/2} \quad (23)$$

From the obtained partial derivatives, the uncertainty of energetic efficiency can be calculated as shown below;

$$w_{\eta_I} = \left[\left(\frac{v_{dch}}{v_{ch}(T_{in,ch} - T_{out,ch})} \times w_{T_{out,dch}} \right)^2 \right. \tag{24}$$

$$+ \left(\frac{-v_{dch}}{v_{ch}(T_{in,ch} - T_{out,ch})} \times w_{T_{in,dch}} \right)^2$$

$$+ \left(\frac{-v_{dch}(T_{out,dch} - T_{in,dch})(-v_{ch})}{(v_{ch} \times T_{in,ch} - v_{ch} \times T_{out,ch})^2} \times w_{T_{out,ch}} \right)^2$$

$$+ \left(\frac{-v_{dch}(T_{out,dch} - T_{in,dch})(v_{ch})}{(v_{ch} \times T_{in,ch} - v_{ch} \times T_{out,ch})^2} \times w_{T_{in,ch}} \right)^2$$

$$+ \left(\frac{T_{out,dch} - T_{in,dch}}{v_{ch}(T_{in,ch} - T_{out,ch})} \times w_{T_{in,ch}} \right)^2$$

$$\left. + \left(\frac{v_{dch}(T_{out,dch} - T_{in,dch})}{T_{in,ch} - T_{out,ch}} \times \frac{-1}{{v_{ch}}^2} \times w_{m_{ch}} \right)^2 \right]^{1/2}$$

The uncertainty of the calculated exergetic efficiency is obtained in a similar way. The uncertainties of the calculated energetic and exergetic efficiencies are shown in Table 5.

Chapter 4

EXPERIMENTAL STUDY

4.1 Material Selection and Synthesis

The selected salts in this study are $CaCl_2$, LiCl, $MgCl_2$, $LiNO_3$, and the mixture $CaCl_2$-LiCl, and they are extensively used as a sorption material in THS systems because they are highly hygroscopic. In addition, the targeted host matrices in this study are pumice and vermiculite. The porous host matrices are impregnated with composite salts to produce a composite sorbent. These host matrices have significant importance on the overall absorption/desorption mechanism. Vermiculite is used as a porous composite in THS systems due to its low charging temperature and low price [3], [7]. It also prevents the composite salt from seeping out during the discharge process. Pumice is a host porous matrix used widely as an insulation material in energy-efficient buildings.

The nine prepared sorption materials are P-$CaCl_2$, V-$CaCl_2$, P-LiCl, V-LiCl, P-$MgCl_2$, V-$MgCl_2$, P-$LiNO_3$, V-$LiNO_3$, and P-$CaCl_2$-LiCl. Initially, 44.7wt% $CaCl_2$, 45.6wt% LiCl, 35wt% $MgCl_2$, and 47wt% $LiNO_3$ salts were prepared for the preparation of the nine sorbents and a mixture of $CaCl_2$-LiCl with a ratio of 50:50% (mass basis). Then, pumice and vermiculite were dried in the oven at 150 °C to ensure that the material was totally dried and ready for impregnation. Then, the dried pores of pumice and vermiculite were impregnated with salts solution. To ensure that the materials are saturated, the impregnation of host matrices continue until some solution is leaked out

of the material. After that, the materials were dried in the oven at a temperature of 150 °C to remove all the water, and only dry salt crystals remained inside the pores of pumice and vermiculite. In the end, dried composite materials (totally charged materials) were stored in sealed containers to prevent them from absorbing moisture until the beginning of their testing. The synthesize procedure applied for preparing the materials is illustrated in Figure 5.

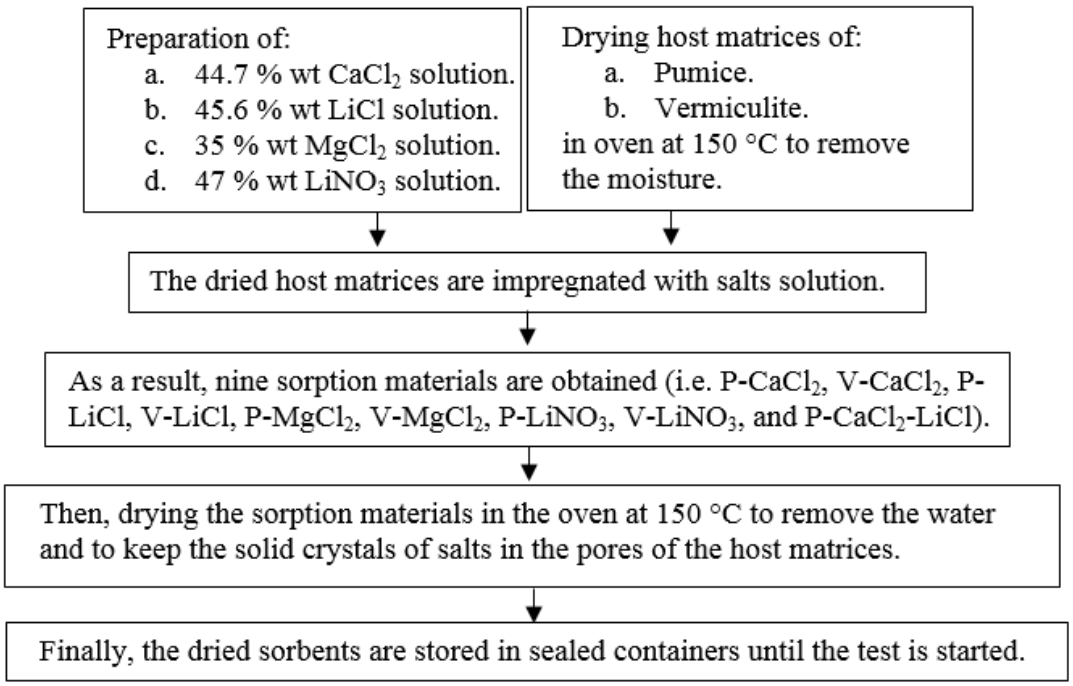

Figure 5: Sorption Material Synthesize Procedure.

4.2 Devices Used for Data Collection

During the experiment, the Sensirion SHTC3 sensor (see Figure 6a) was used to measure the ambient/inlet/outlet temperature and relative/absolute humidity with a typical accuracy of ± 0.2%°C and ± 2% RH. In addition, Xplorer GLX weather anemometer (see Figure 6b) was used to measure the velocity of air at the reactor's exit and to measure and record the temperatures as a backup. Additionally, a desktop

computer connected with Sensirion SHTC3 was used to store the collected data. The standard accuracy and error of instruments are shown in Table 2.

Figure 6: (a) Sensirion SHTC3 Sensor, and (b) Xplorer GLX Weather Anemometer

Table 2: Standard Measuring Range, Accuracy, and Error of Apparatus.

Sensor	Measured parameter	Range	Error	Accuracy
Sensirion SHTC3	Temperature	0 – 140 °C	± 1.2 %	± 0.2 °C
	Relative humidity	0 – 100 %	± 2.5 %	± 2.0 %
Xplorer-GLX Anemometer	Air velocity	1 – 7 m/s	± 3.0 %	± 0.1 m/s

4.3 Experimental Setup

The view of the experimental THS prototype is shown in Figure 7. The wire mesh tray used in the experiments and the electric furnace are illustrated in Figure 8a and 8b, respectively. The experimental setup contains an air-conditioning unit with two electric heaters, one radial fan, and two household humidifiers. Additionally, it includes a rectangular-shaped reactor with a wire mesh tray. Computer and data

loggers are used in the experimental setup. The purposes of the main components of the THS prototype are explained below in detail;

- The fan is used for blowing the ambient air into the system.
- The air-conditioning unit is used for supplying desired inlet air during the discharging and charging operations to the reactor, and it is used for heating the inlet air during the charging process by electric heaters.
- Humidifiers are used to humidify the inlet air during the discharging process.
- A reactor is used to place composite material within the wire mesh tray during discharging and charging processes.
- Computer and sensors are used for recording and analyzing data.

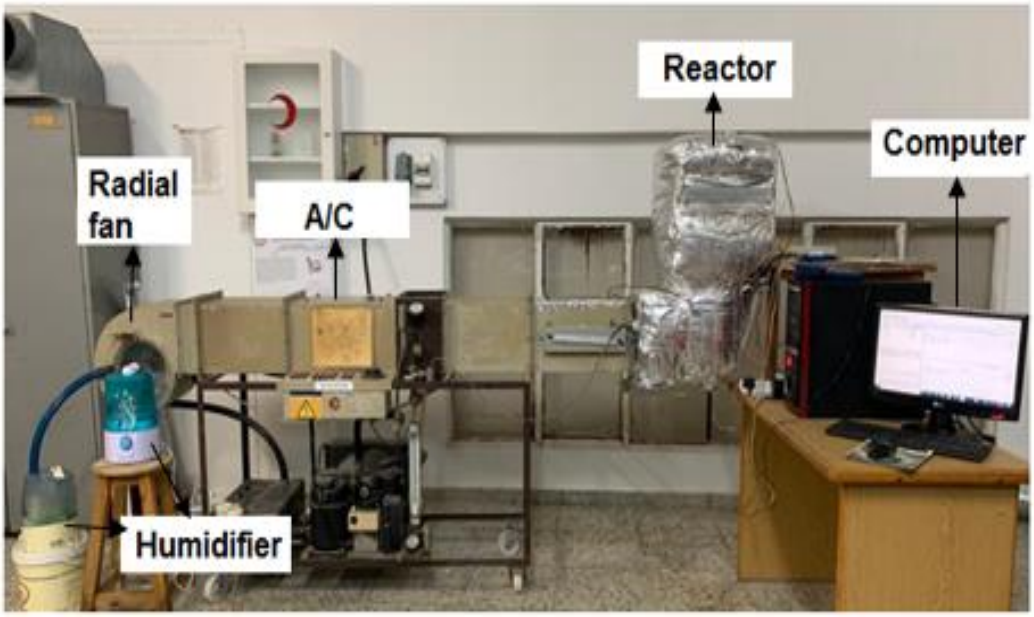

Figure 7: Overall View of the Experimental THS Prototype.

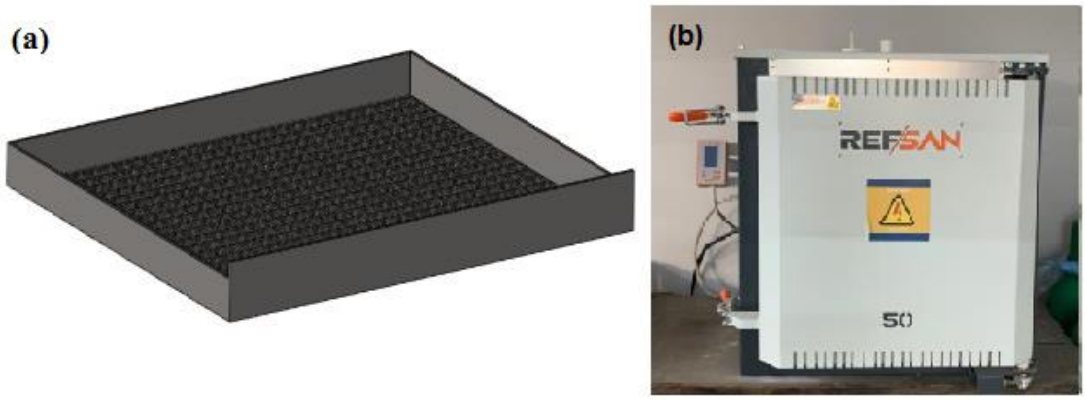

Figure 8: (a) Wire Mesh Tray and (b) Electric Furnace.

4.4 Experimental Methodology

Figure 9 depicts the fundamental representation of the discharging/charging cycles described in this experimental investigation. The testing methodology used in this investigation is presented in Figure 10. After synthesizing the composite materials, sorbents were tested over four discharging and charging cycles. With the repeating cycles we can identify the cyclic stability and performance of materials.

The discharging cycles was performed for 90 minutes under the conditions of $T_{in} = 19 - 23$ °C and $RH_{in} = 80 - 85$ %. In charging, the cycles were also performed for 90 minutes (same as discharging cycles) under the conditions of $T_{in} = 80 - 85$ °C. The temperatures, relative humidity, and mass changes were measured over testing time. By using the recorded data of discharging/charging cycles, performance parameters such as velocity, average temperature, heat, cumulative energy, exergy, cumulative exergy, sorption/desorption rates and energy storage density were calculated. Moreover, based on the results obtained from discharging and charging cycles, energetic, exergetic and hygrothermal efficiencies were calculated.

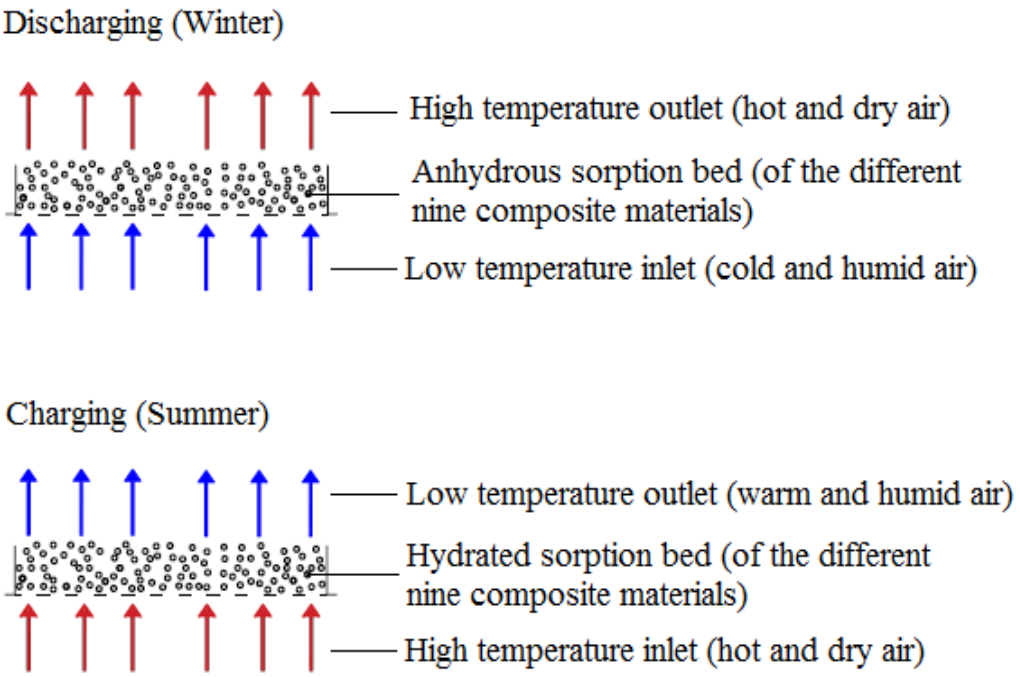

Figure 9: Basic Illustration of Sorption and Desorption Cycles.

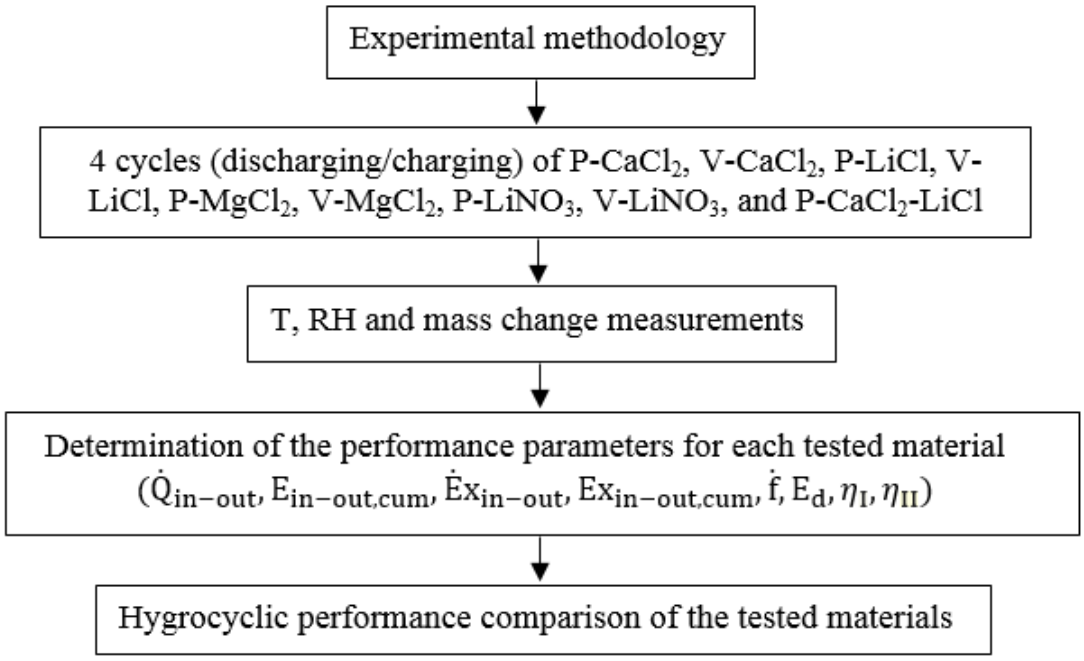

Figure 10: Experimental Methodology Applied in this Study.

Chapter 5

RESULTS AND DISCUSSION

5.1 Discharging Analysis

The experimental study was carried out with four repeating cycles under laboratory conditions in North Cyprus. In this part, the characteristics of P-$CaCl_2$, V-$CaCl_2$, P-LiCl, V-LiCl, P-$MgCl_2$, V-$MgCl_2$, P-$LiNO_3$, V-$LiNO_3$, and P-$CaCl_2$-LiCl were investigated for four discharging cycles. The duration of each discharging process was 90 minutes, and the mass flow rate of air during the discharging phase was measured and calculated differently for every cycle and material. Percentage errors and ranges accuracies of the measuring instruments used are shown in Table 2.

5.1.1 Energy Analysis

The outlet air temperature variations for the tested nine sorption materials over the number of cycles are shown in Figure 11. The inlet air temperature was measured around 19-23 °C, affected by the fluctuating room temperature during the experiment. Due to the high sorbate absorption rate, all nine sorbent materials showed significant temperature rise at the start of each cycle. All of the sorbents (P-$CaCl_2$, V-$CaCl_2$, P-LiCl, V-LiCl, P-$MgCl_2$, V-$MgCl_2$, and P-$CaCl_2$-LiCl) show average outlet temperature in the range of 40 – 30 °C in the first cycle, except P-$LiNO_3$ and V-$LiNO_3$ that shows $T_{out,avg} = 28 - 23\,℃$. P-$CaCl_2$, P-LiCl, and P-$CaCl_2$-LiCl show a very high steady performance among other sorbents during the repeating cycles. P-$CaCl_2$ has a high outlet temperature (44 – 38 °C) at the beginning of each cycle and then decreases during the 1^{st},2^{nd}, 3^{rd}, and 4^{th} by 33, 27, 20, and 30 %, respectively to reach around 29

°C at the end. P-LiCl shows the highest outlet average temperature of 37, 33, 33, and 34 °C over the repeating four cycles, respectively. The mixture composite material (P-$CaCl_2$-LiCl) showed almost similar outlet average temperature of P-$CaCl_2$ and P-LiCl, the average temperature was found as 33, 29, 29, and 29 °C during the four cycle. Therefore, the difference in temperature (ΔT_{avg}) of P-$CaCl_2$ for four cycles was found as 11, 8, 9, and 8 °C, and for P-LiCl, it was 15, 10, 10, and 10 °C, and for P-$CaCl_2$-LiCl, it was 13, 9, 9, and 8 °C for four successive cycles. Thus, the P-$CaCl_2$, P-LiCl, and P-$CaCl_2$-LiCl shows almost similar ΔT_{avg} in the 2nd, 3rd, and 4th cycles.

For V-$CaCl_2$, a very high average outlet temperature was produced during the first cycle with 40 °C, and then followed with 33.8 °C in the 2nd cycle. In addition, the V-$CaCl_2$ dropped sharply in the 3rd and 4th cycles to $T_{avg} = 25$ °C due to the high amount of moisture absorbed in the first and second cycles, which negatively influenced the material structure in the third and fourth cycles. As, $CaCl_2$ (which has a high absorption rate) absorbed a high amount of moisture, vermiculite is damaged and it became muddy due to its spongy structure. In V-LiCl, the average outlet temperature decreased continuously by 16 % from the first to fourth cycle (42°C to 35 °C) due to less amount of moisture is removed from material during charging cycle (more charging time is needed). Therefore, ΔT_{avg} of V-$CaCl_2$ for four cycles was found as 19, 11, 3, and 3 °C, and for V-LiCl, it was 20, 18, 15, and 11 °C, for four successive cycles.

With P-$MgCl_2$, it produced heat with an average temperature of 31, 27, 28, and 27 °C within the four cycles, and it shows a steady performance during the 2nd, 3rd, and 4th cycles. Similarly, V-$MgCl_2$ offers stable performance in the last three cycles with an average outlet temperature of (34, 28, 27, and 27 °C during the four cycles). For four

cycles, the ΔT_{avg} of P-$MgCl_2$, was 8, 5, 6, and 5 °C, whereas the ΔT_{avg} of V-$MgCl_2$ was 13, 8, 8, and 7 °C. P-$LiNO_3$ and V-$LiNO_3$ show an increase in the average outlet temperature during the four cycles because the containers were not sealed well in which the materials absorbed some moisture from the air before testing them. Additionally, the materials were charged well during the charging cycles, so their average outlet temperature increased within the discharging processes. Therefore, the average outlet temperatures of P-$LiNO_3$ were found as (23, 25, 27, and 28 °C), and V-$LiNO_3$ were recorded as (28, 30, 29, and 31 °C). Furthermore, the ΔT_{avg} of P-$LiNO_3$ for four cycles was found as 5, 5, 6, and 7 °C, and for V-$LiNO_3$, it was 8, 10, 10, and 11 °C, for four successive cycles.

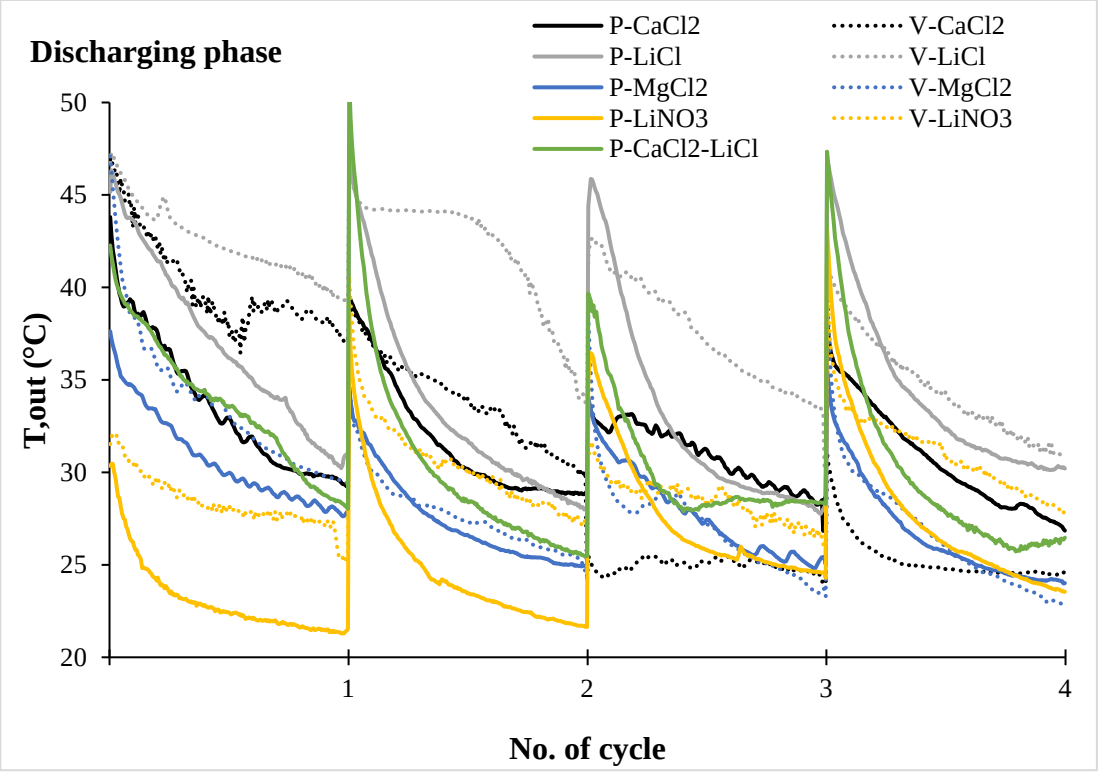

Figure 11: Outlet Temperature Variations of Nine Sorption Materials over Four Discharging Cycles.

Relative humidity (RH) variations of outlet air over-discharging period are illustrated in Figure 12. The RH of air varied between 80-85 % at the inlet of the reactor and 5-

60 % at the outlet of the reactor. Therefore, some of the sorbents show a high amount of RH absorbed, where it reached ~73 % at the beginning of the experiment, and most of the materials gradually drop to 60 – 40 % and almost stay constant in the 2nd, 3rd, and 4th cycles.

The variation of ΔRH in P-$CaCl_2$ for four cycles was found as 54, 42, 47, and 41 %, and for P-LiCl, it was 66, 48, 50, and 49 %, and for P-$CaCl_2$-LiCl, it was 56, 45, 46, and 43 %. Thus, the P-$CaCl_2$, P-LiCl, and P-$CaCl_2$-LiCl shows almost similar ΔRH_{avg} in the 2nd, 3rd, and 4th cycles. In addition, the ΔRH_{avg} of V-$CaCl_2$ for four cycles was found as 73, 60, 24, and 24 %, and for V-LiCl, it was 71, 66, 69, and 57 % for four successive cycles. Therefore, V-$CaCl_2$ and V-LiCl show the highest ΔRH in all cycles compared to other sorbents, except in the 3rd and 4th cycles of V-$CaCl_2$, where ΔRH_{avg} dramatically drops because the material was damaged due to high sorption rate of moisture in previous cycles. Additionally, during the four cycles, the ΔRH_{avg} of P-$MgCl_2$, was 46, 37, 40, and 36 %, whereas of V-$MgCl_2$ was 62, 49, 51, and 44 %.

The ΔRH_{avg} of P-$LiNO_3$ was found as 37, 36, 39, and 45 %, and for V-$LiNO_3$, it was 51, 59, 61, and 63 %, for four successive cycles. Thus, the ΔRH_{avg} are increased within the cycles with P-$LiNO_3$ and V-$LiNO_3$ because the sorbents were not charged well before starting the 1st and 2nd cycles (the materials were not sealed well in the containers).

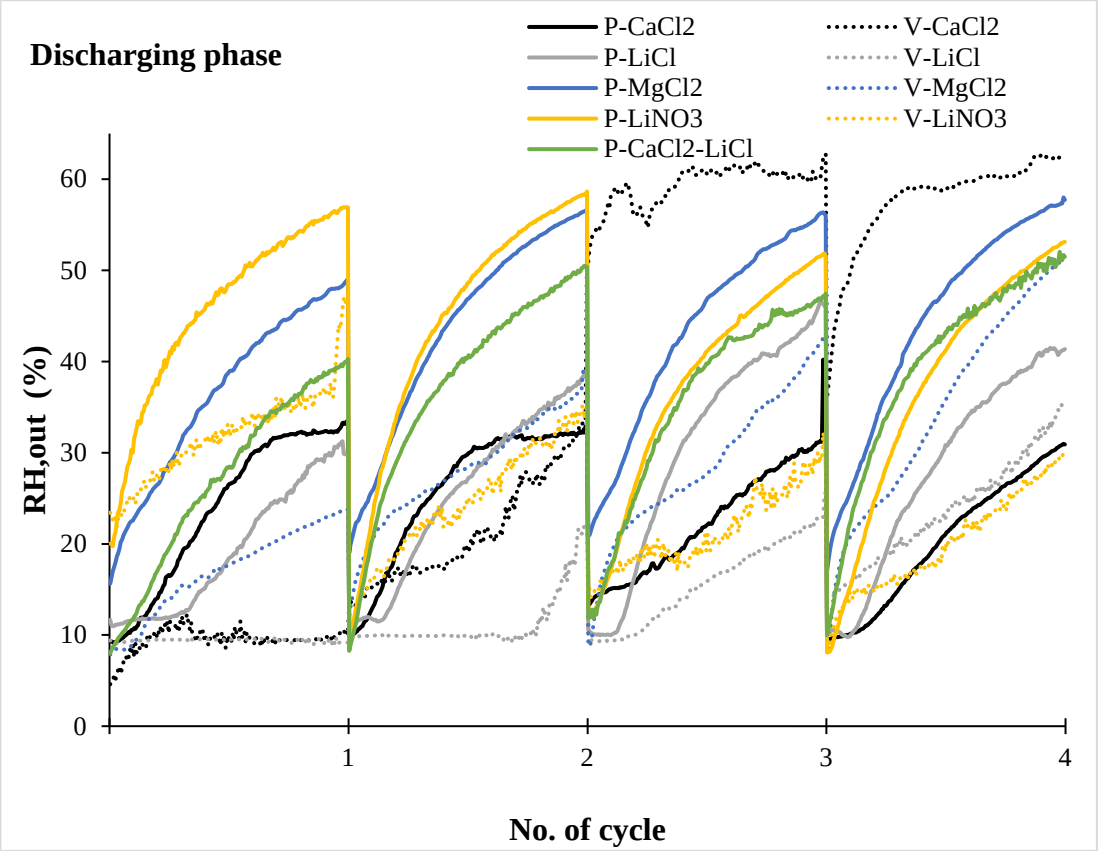

Figure 12: Output Relative Humidity Variations of Nine Sorption Materials over Four Discharging Cycles.

The energy outlets of the sorbents over the discharging processes are illustrated in Figure 13. The average outlet heat flow rate of P-$CaCl_2$ was 0.69, 0.53, 0.52, and 0.53 kW in each cycle, respectively. Energy outlet of P-LiCl was 0.83, 0.62, 0.56, and 0.58 kW, and of P-$CaCl_2$-LiCl was 0.77, 0.57, 0.52, and 0.50 kW. The total energy output of V-$CaCl_2$ and V-LiCl decreased considerably in each cycle due to poor desorption of vapor in the charging cycle and were 0.90, 0.44, 0.16, 0.10 kW, and 1.15, 1.10, 0.85, 0.69 kW over four repeating cycles respectively. In fact, the highest energy outlet among all the material was with V-LiCl over the four cycles. For P-$MgCl_2$ and V-$MgCl_2$, heat outlet rate were 0.48, 0.35, 0.35, 0.31 kW, and 0.70, 0.48, 0.57, 0.41 kW over four repeating cycles respectively. Additionally, the outlet heat flow rate (energy output) of P-$LiNO_3$ and V-$LiNO_3$ in each cycle increased and was, 0.22, 0.28, 0.30, 0.35 kW, and 0.30, 0.36, 0.40, 0.48 kW, respectively. Moreover, the increase of the

outlet heat flow rate in P-$LiNO_3$ and V-$LiNO_3$ was due to the rise of the ΔT_{avg} over repeating cycles.

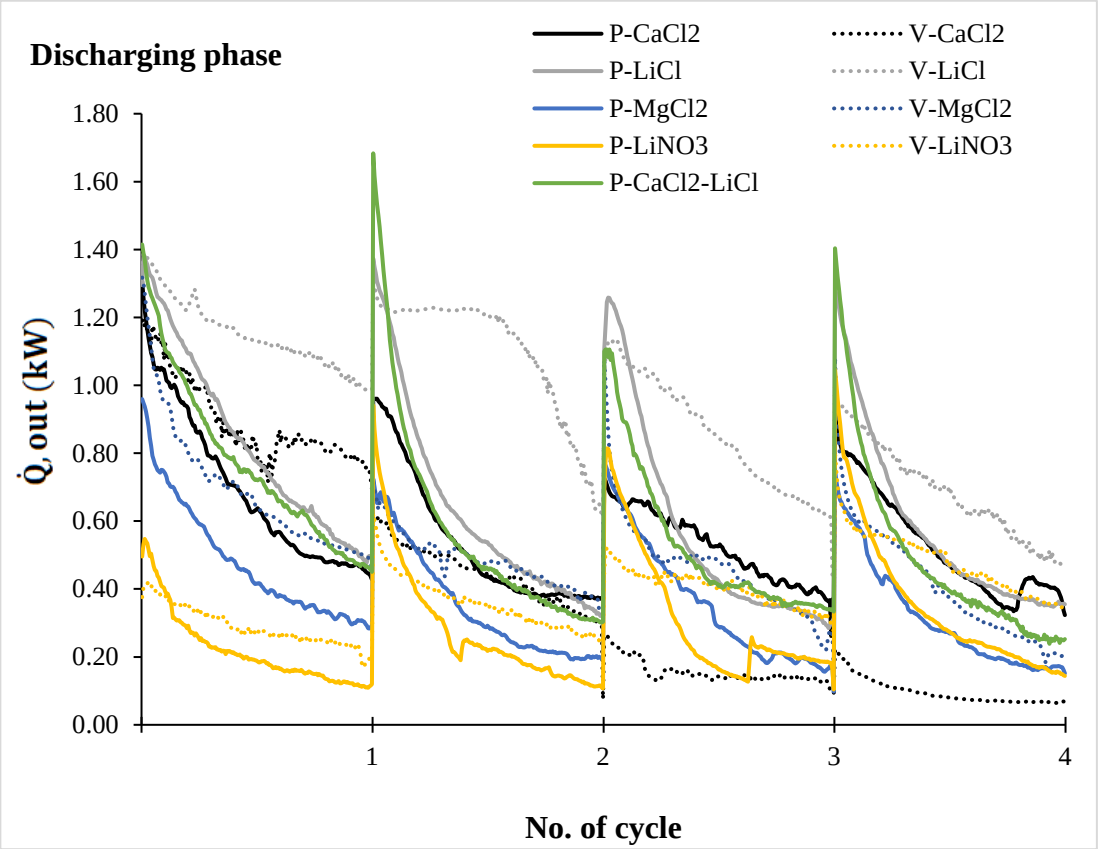

Figure 13: Output Energy Rate Variations of Nine Sorption Materials over Four Discharging Cycles.

The energy density of nine sorption materials in discharging processes are illustrated in Figure 14. The energy densities of P-$CaCl_2$, P-LiCl, and P-$CaCl_2$-LiCl were found as 296, 228, 224, 225 kWh/m^3, 356, 267, 240, 247 kWh/m^3, and 329, 244, 224, 210 kWh/m^3 over four repeating cycles, respectively. The energy density of V-$CaCl_2$ was 383, 189, 67, and 41 kWh/m^3. In addition, the highest energy density among all materials was found in V-LiCl, with 492, 471, 364, and 294 kWh/m^3. In P-$MgCl_2$ and V-$MgCl_2$, the energy density was 205, 148, 152, 134 kWh/m^3, and 296, 206, 197, 176 kWh/m^3 over four cycles, respectively. Moreover, for P-$LiNO_3$ and V-$LiNO_3$, the

energy density was found as 94, 119, 132, 150 kWh/m^3, and 124, 153, 172, 205 kWh/m^3, respectively.

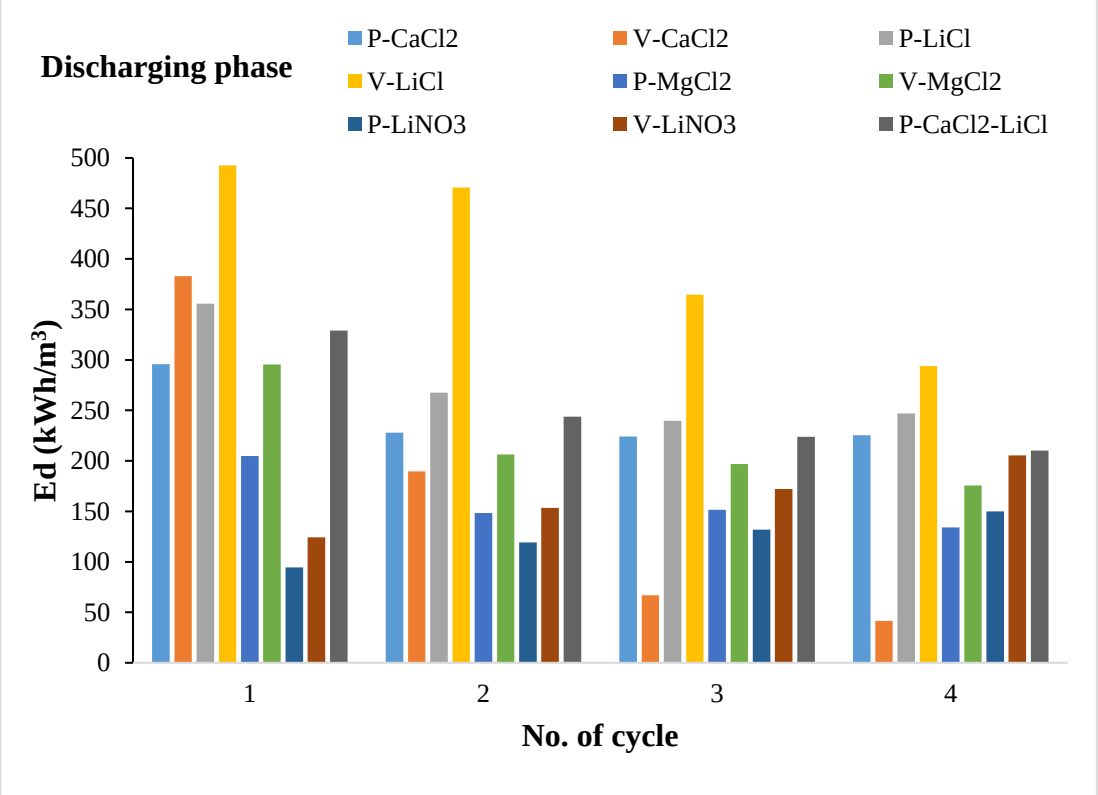

Figure 14: Energy Density of Nine Sorption Materials over Four Discharging Cycles.

5.1.2 Exergy Analysis

Exergy output rate ($\dot{E}x, out$) variations over-discharging phase are presented in Figure 15. The exergy output profiles for the studied materials differ from the energy output profiles. For P-$CaCl_2$, P-LiCl and P-$CaCl_2$-LiCl, exergy outputs were 0.008, 0.004, 0.004, 0.004 kW, 0.015, 0.008, 0.007, 0.006 kW, and 0.013, 0.007, 0.006, 0.006 kW over four repeating cycles respectively. Thus, the exergy rates are steadier in the 1st, 2nd, and 3rd cycles, but in general, P-LiCl shows the highest exergy rate among the three materials. With P-$CaCl_2$-LiCl, the main reason for the high increase in exergy rate at the beginning of the second and fourth cycles might be described by the fluctuations of ambient temperatures during the experimental test. The exergy output

rate of V-$CaCl_2$ decreased considerably in each cycle due to high ΔT_{avg} drop and was 0.022, 0.005, 0, and 0 kW, over four repeating cycles respectively. In addition, V-LiCl shows the highest Ėx, out compared to other tested materials, and it was 0.028, 0.023, 0.016, and 0.008 kW, but it decreases gradually over the cycles due to the decrease in ΔT_{avg}, and the reduce in ΔT_{avg} is because of insufficient desorption of water in the charging phase.

For P-$MgCl_2$ and V-$MgCl_2$, exergy rates were 0.003, 0.001, 0.002, 0.001 kW, and 0.011, 0.003, 0.004, 0.002 kW over cycles respectively. Therefore, P-$MgCl_2$ shows the lowest exergy rate among the nine sorbents. Additionally, V-$MgCl_2$ shows a dramatic drop in exergy rate from the 1st to 2nd cycle, and this is because of the performance of $MgCl_2$. Moreover, the exergy rates of P-$LiNO_3$ and V-$LiNO_3$ in each cycle increased and were, 0.001, 0.001, 0.002, 0.004 kW, and 0.002, 0.003, 0.004, 0.005 kW, over four cycles respectively.

Exergy is known as useful or potential work, and in heat storage systems, it is important as it provides information on the quality of the heat generated. As a result, the exergy rate was found to be lower than the heat outflow, as was predicted. Moreover, V-LiCl shows the highest exergy outlet rate with 70 % more than most of the tested materials, and this shows that LiCl salt has high performance in all terms found during the experimental study.

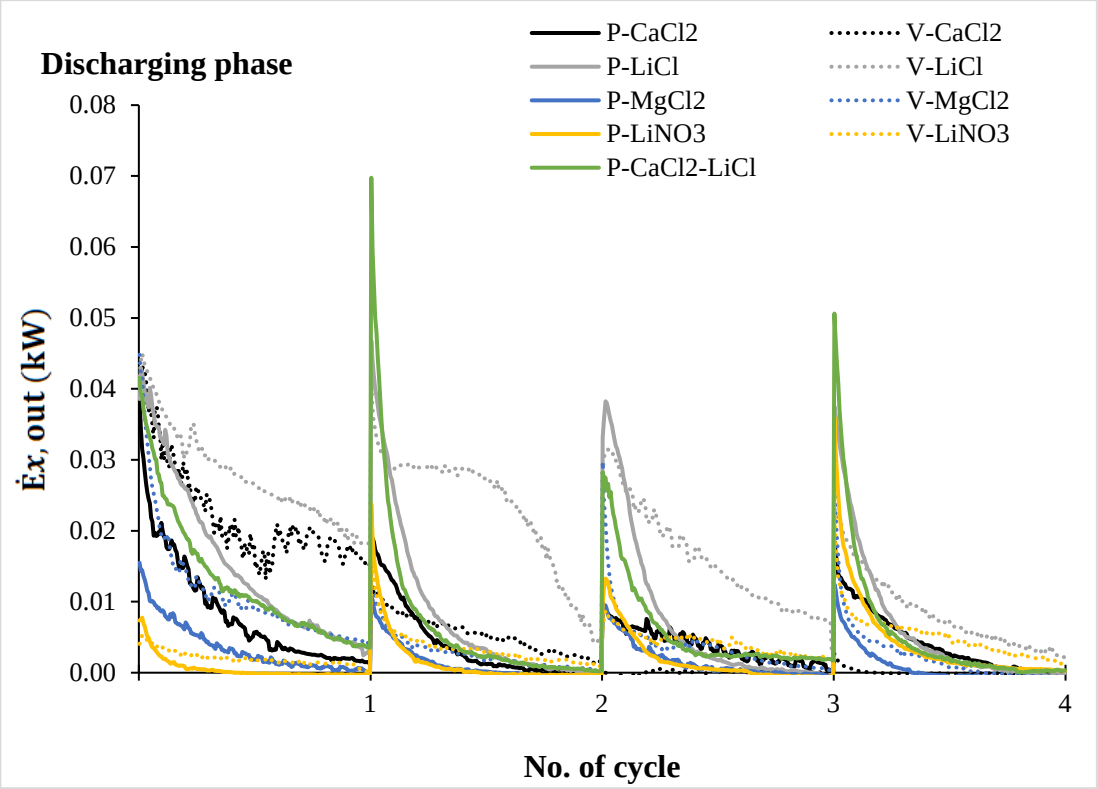

Figure 15: Output Exergy Rate of Nine Sorption Materials over Four Discharging Cycles.

5.1.3 Moisture Sorption Analysis

View of sorption rates ($\dot{f}_{sorp}$) during the discharging cycles of nine sorbents were presented in Figure 16. The amount of sorption rates of moisture for P-$CaCl_2$, P-LiCl and P-$CaCl_2$-LiCl were 0.13, 0.10, 0.10, 0.09 g/s, 0.14, 0.10, 0.12, 0.12 g/s, and 0.13, 0.10, 0.10, 0.10 g/s over four discharging cycles respectively. Therefore, the above three pumice salts show almost the same moisture sorption rate and are constant over cycles. V-$CaCl_2$ shows a high sorption rate in the 1st and 2nd cycles, and then it dramatically drops to 90 %, from 0.16 g/s in the 1st cycle to 0.01 g/s in the 4th cycle, and this is because of the material structural degradation. V-LiCl showed the highest moisture absorption rate among all the materials and was found as 0.20, 0.15, 0.12, and 0.07 g/s. For P-$MgCl_2$ and V-$MgCl_2$, sorption rates were found almost constant in all cycles as 0.08, 0.07, 0.07, 0.07 g/s, and 0.11, 0.10, 0.10, 0.10 g/s. The lowest

sorption rate was found in P-$LiNO_3$ with 0.06, 0.05, 0.04, and 0.05 g/s. V-$LiNO_3$ shows a constant moisture sorption rate of 0.08 g/s. Moreover, all the materials except V-$CaCl_2$ and V-LiCl show a constant sorption rate in the 2nd, 3rd, and 4th cycles.

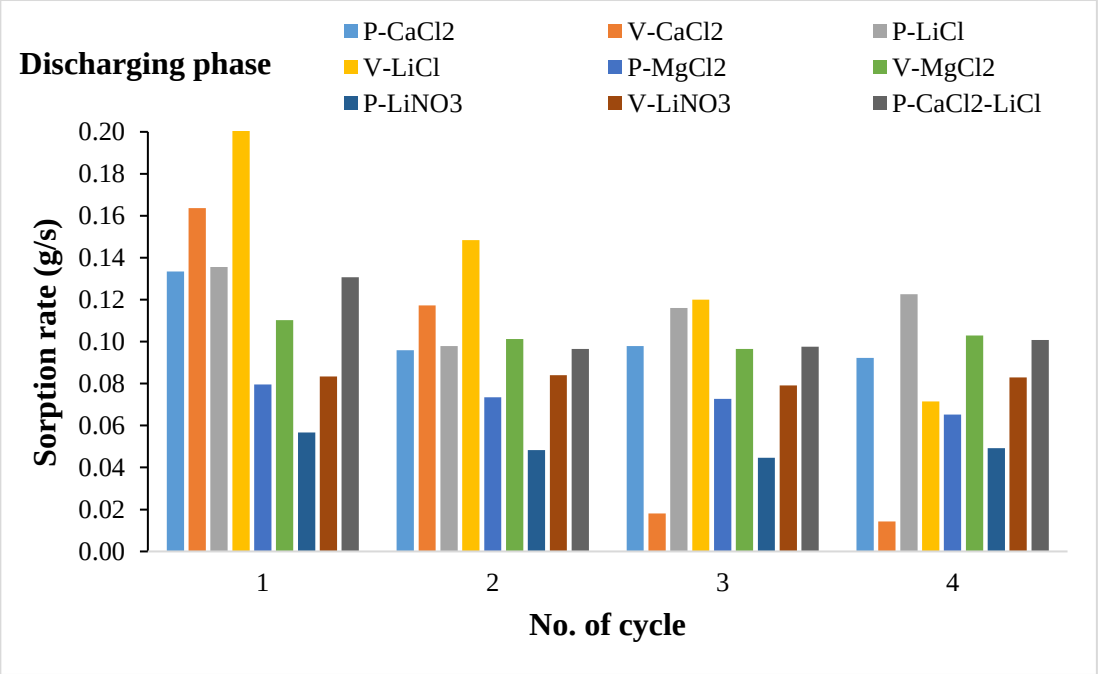

Figure 16: Sorption Rate of Nine Sorption Materials over Four Discharging Cycles.

Heat output per sorption rate profiles of the nine THS materials are presented in Figure 17. P-$CaCl_2$ shows a constant heat output per gram of vapor with an average of 5.44 kJ/g over the four cycles. Both P-LiCl and P-$CaCl_2$-LiCl have almost the same outlet heat rate per sorption rate in each process and was, respectively, 6, 6, 5, and 5 kJ/g. In terms of less sorption rate in the 3rd and 4th cycles with V-$CaCl_2$, there was a high outlet heat rate. V-LiCl showed the highest heat outlet rate per gram of sorption of vapor among all the sorbents and was increased gradually over the cycles and found as 6, 7, 7, and 10 kJ/s. Both P-$MgCl_2$ and V-$MgCl_2$ almost showed constant and same heat outputs per sorption rates and were 6, 5, 5, 5 kJ/g, and 6, 5, 5, 4 kJ/g over four discharging cycles, respectively. Heat outlets per sorption rates of P-$LiNO_3$ and V-

$LiNO_3$ increased gradually in each cycle, and were respectively, 4, 6, 7, 7 kJ/g, and 3, 4, 5, 6 kJ/g.

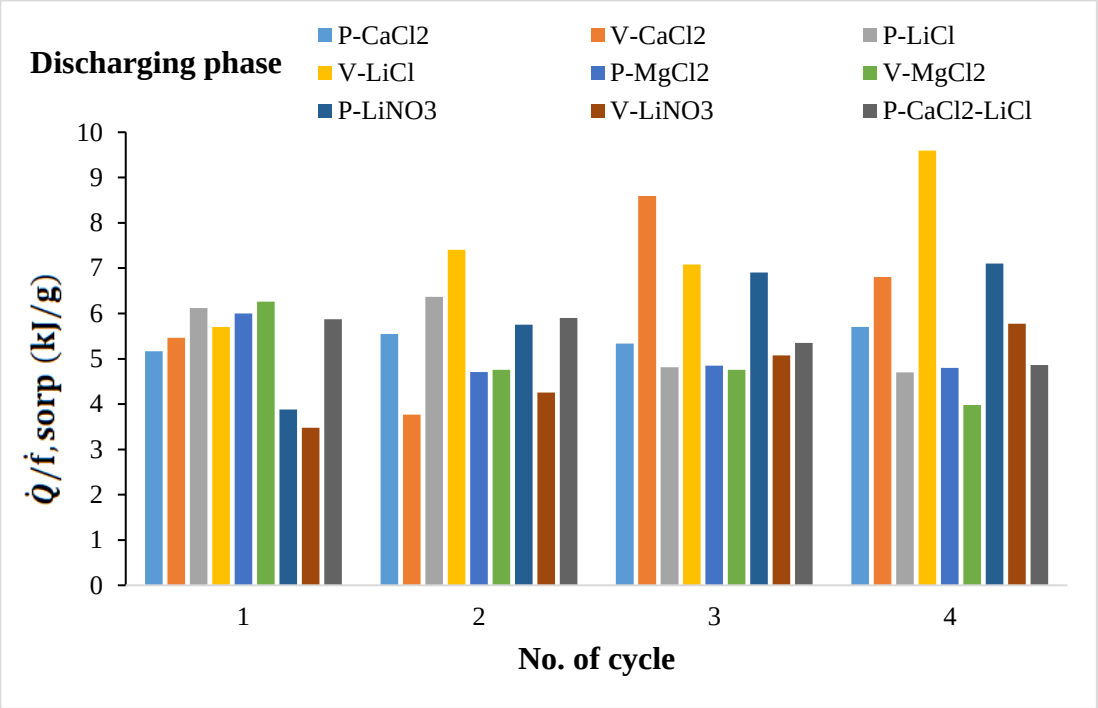

Figure 17: Heat Outlet Rate per Sorption Rate of Nine Sorption Materials over Four Discharging Cycles.

Exergy outlet rate per sorption rate ($\dot{E}x/\dot{f}_{sorp}$) profiles of nine sorbents in discharging processes are illustrated in Figure 18. P-$CaCl_2$ shows a constant exergy per sorption rate, and it was 0.06, 0.04, 0.04, and 0.04 kJ/g. Both P-LiCl and P-$CaCl_2$-LiCl have almost same outlet exergy rate per sorption rate in each cycle and was, respectively, 0.11, 0.08, 0.06, 0.05 kJ/g, and 0.10, 0.07, 0.06, 0.06 kJ/g. For V-$CaCl_2$, it shows the high output $\dot{E}x/\dot{f}_{sorp}$ in the first cycle with 0.13 kJ/g, and then it dramatically drops to zero kJ/g in the 3rd and 4th cycles. The highest exergy outlet per gram of moisture sorption was in V-LiCl, and it was 0.14, 0.16, 0.13, and 0.11 kJ/g over four cycles respectively. Thus, V-LiCl shows the highest performance of all parameters among all materials. In addition, the $\dot{E}x/\dot{f}_{sorp}$ of P-$MgCl_2$ and V-$MgCl_2$ was low compared to

other sorbents, and a result found as 0.04, 0.01, 0.03, 0.02 kJ/g, and 0.10, 0.03, 0.04, 0.02 kJ/g over four discharging cycles respectively. Exergy outlets per sorption rates of P-$LiNO_3$ and V- $LiNO_3$ increased gradually in each cycle, and were respectively, 0.02, 0.02, 0.04, 0.08kJ/g, and 0.02, 0.04, 0.05, 0.06kJ/g.

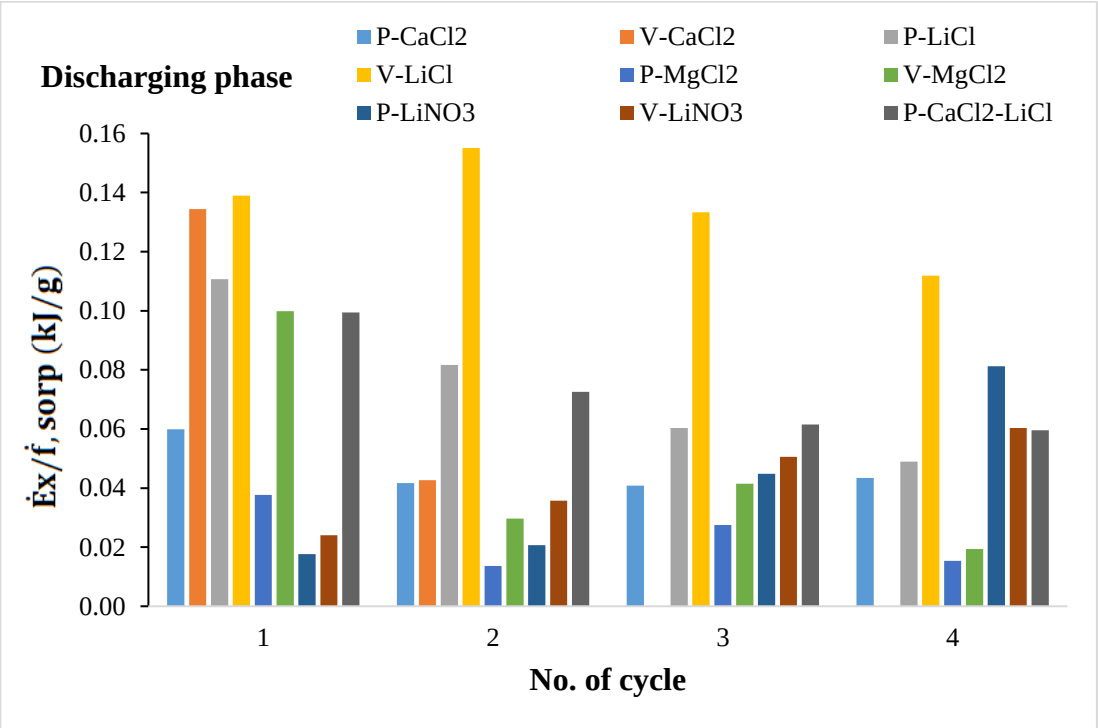

Figure 18: Exergy Outlet Rate per Sorption Rate of Nine Sorption Materials over Four Discharging Cycles.

5.2 Charging Analysis

The four cycles charging characteristics of P-$CaCl_2$, V-$CaCl_2$, P-LiCl, V-LiCl, P-$MgCl_2$, V-$MgCl_2$, P-$LiNO_3$, V-$LiNO_3$, and P-$CaCl_2$-LiCl, with $t_{ch} = 90$ min are analyzed in this section. Air mass flow rate was found differently for every cycle and material because of different velocity measurements.

5.2.1 Energy Analysis

The outlet temperature variations of air during the charging process of nine sorbents are presented in Figure 19. During the charging cycles, the inlet temperature of the air was in the range of 80-85 °C, affected by the surrounding weather condition during the experimental test. The average outlet of the temperature of all sorbents was between 59-72 °C. The ΔT_{avg} for P-$CaCl_2$, P-LiCl and P-$CaCl_2$-LiCl over four charging cycles were 16, 13, 13, 12°C, 16, 15, 18, 18°C, and 14, 13, 13, 12°C, respectively. Thus, the conditions show that P-$CaCl_2$, P-LiCl, and P-$CaCl_2$-LiCl release moisture at a steady rate, which means the materials have good charging characteristics. As shown in Figure 19, V-$CaCl_2$ shows a high outlet temperature in the 3rd and 4th cycles, and this is because of the material structural degradation where no moisture is removed in the last two cycles. Thus, the inlet heat is almost the same as the heat outlet for V-$CaCl_2$ in the charging phase. For V-LiCl, the material shows the lowest outlet of temperature compared to other materials with an average of 62 °C in the four cycles, which means that the material needs more time to be charged well, additionally, it also shows the highest outlet ΔT_{avg} with an average of 20 °C. During the four cycles, the ΔT_{avg} of P-$MgCl_2$, was 13, 9, 11, and 10 °C, whereas the ΔT_{avg} of V-$MgCl_2$ was 13, 13, 13, and 12 °C. In addition, P-$LiNO_3$ shows the lowest outlet of temperature difference (ΔT_{avg}) among all sorbents, which means that P-$LiNO_3$ has good characteristics with charging process, and was 9, 9, 10, and 10 °C, respectively. Therefore, with a low outlet of temperature difference (ΔT_{avg}) there will be a high outlet of temperature ($T_{out,avg}$). Moreover, V- $LiNO_3$ shows an average temperature difference of 13, 13, 15, and 14 °C, over four repeating cycles respectively.

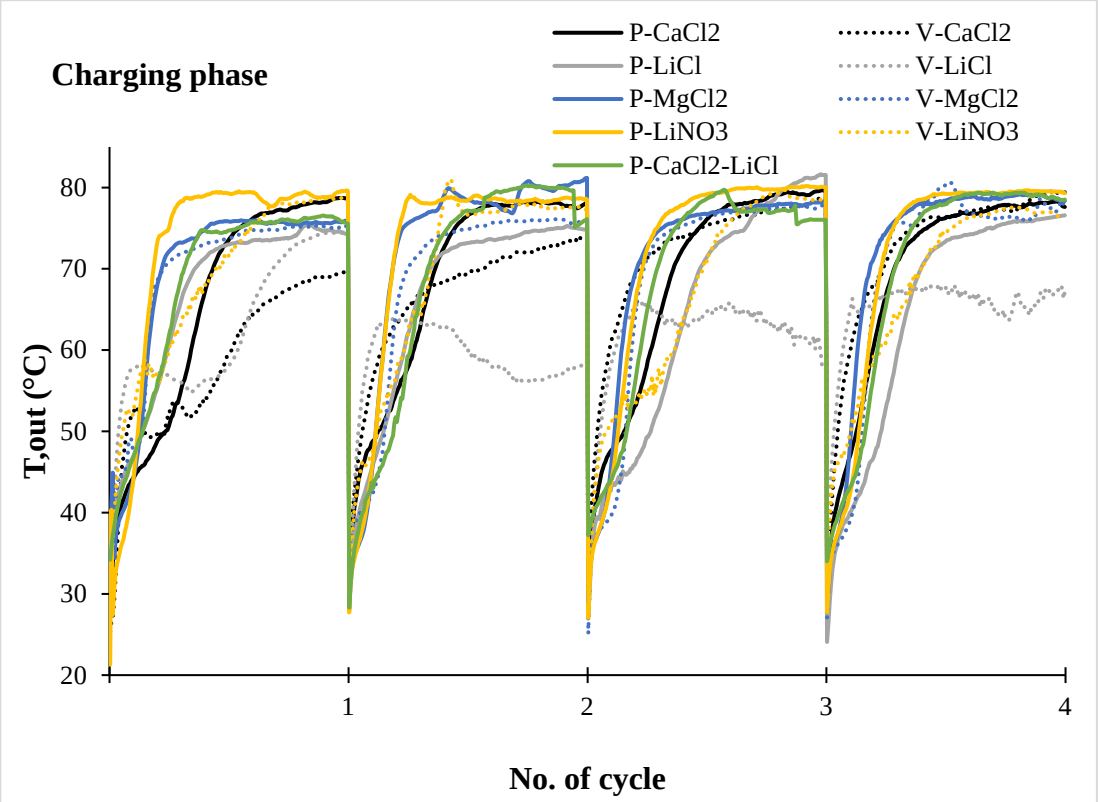

Figure 19: Outlet Temperature Variations of Nine Sorption Materials over Four Charging Cycles.

The relative outlet humidity (RH) variations of air over charging cycles are presented in Figure 20. The outlet RH variations in the charging phase were between 3-60 %. As known, the outlet relative humidity in the beginning of every cycle is high, since high amount of moisture is removed initially from the sorbents in charging process. The ΔRH of P-$CaCl_2$, P-LiCl and P-$CaCl_2$-LiCl over four charging cycles were 10, 9, 8, 7 %, 6, 7, 10, 9 %, and 9, 11, 10, 9 %, respectively. The lowest ΔRH was with V-$CaCl_2$, and found as 6, 6, 4, and 4 % over the four cycles respectively. In addition, the ΔRH in each cycle of V-LiCl was 6, 8, 8, and 6 %, and that shows a decrease in the last cycle due to insufficient charging time. Both P-$MgCl_2$ and V-$MgCl_2$ shows a high ΔRH, and was 7, 8, 8, 7% and 6, 8, 10, 9 %, during four successive cycles. Moreover, P-$LiNO_3$ and V- $LiNO_3$ shows a gradually increase of an ΔRH, and was 8, 8, 9, 9 %, and 6, 7, 8, 7 %.

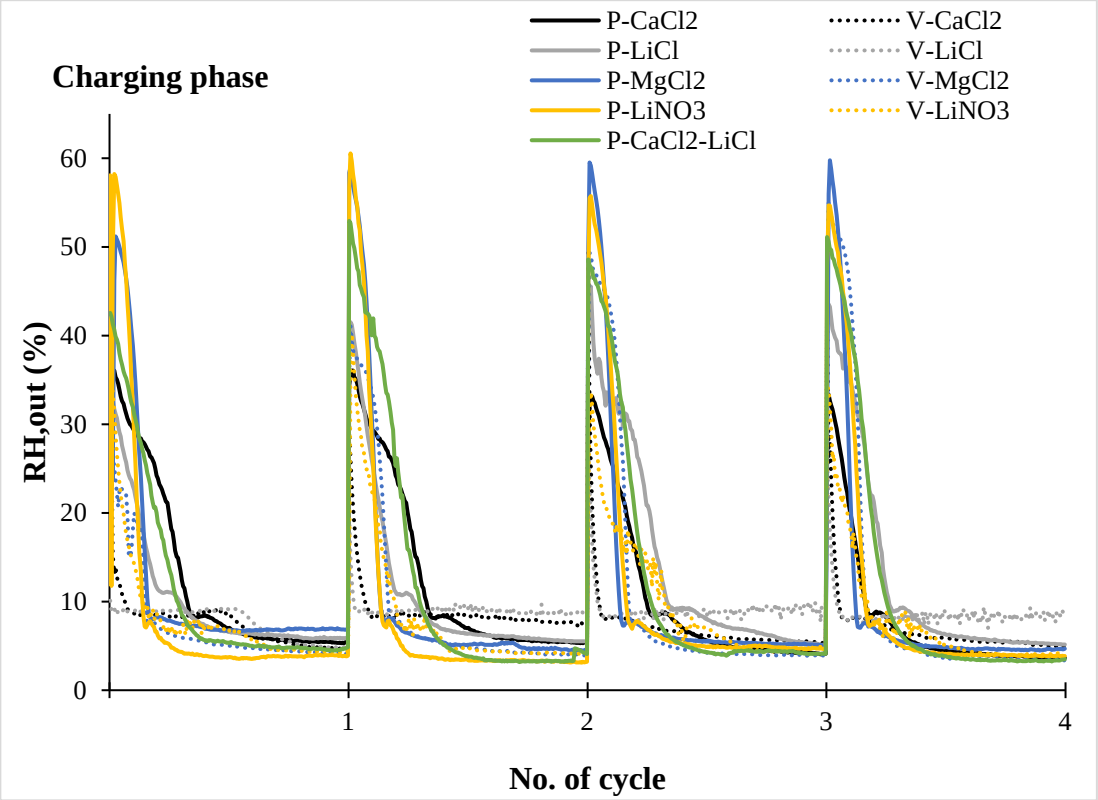

Figure 20: Outlet Relative Humidity Variations of Nine Sorption Materials over Four Charging Cycles.

The THS system's charging cycle energy profiles for P-$CaCl_2$, V-$CaCl_2$, P-LiCl, V-LiCl, P-$MgCl_2$, V-$MgCl_2$, P-$LiNO_3$, V-$LiNO_3$, and P-$CaCl_2$-LiCl are illustrated in Figure 21. The inlet heat flow rate rate of P-$CaCl_2$, P-LiCl and P-$CaCl_2$-LiCl over four charging cycles were 0.97, 0.84, 0.83, 0.77 kW, 0.97, 0.99, 1.03, 1.09 kW, and 0.85, 0.88, 0.82, 0.78kW, respectively. Thus, a gradual increase of inlet energy rate in each cycle was found in P-LiCl. In addition, V-$CaCl_2$ shows a dramatic decrease of inlet energy rate, and was 1.07 kW in the first cycle, and 0.40 kW in the fourth cycle. Additionally, the highest inlet energy among all the test materials was with V-LiCl, and was found as 1.27, 1.53, 1.18, 1.10 kW. For P-$MgCl_2$ and V-$MgCl_2$, heat inlet rate over four repeating cycles were 0.80, 0.60, 0.64, 0.58 kW, and 0.84, 0.87, 0.73, 0.78 kW, respectively. P-$LiNO_3$ shows a constant rate of energy inlet with an average of

0.55 kW for the four cycles. Moreover, V-$LiNO_3$ shows a gradually increase in the rate of heat inlet with 0.46, 0.56, 0.60, and 0.62 kW over charging cycles respectively.

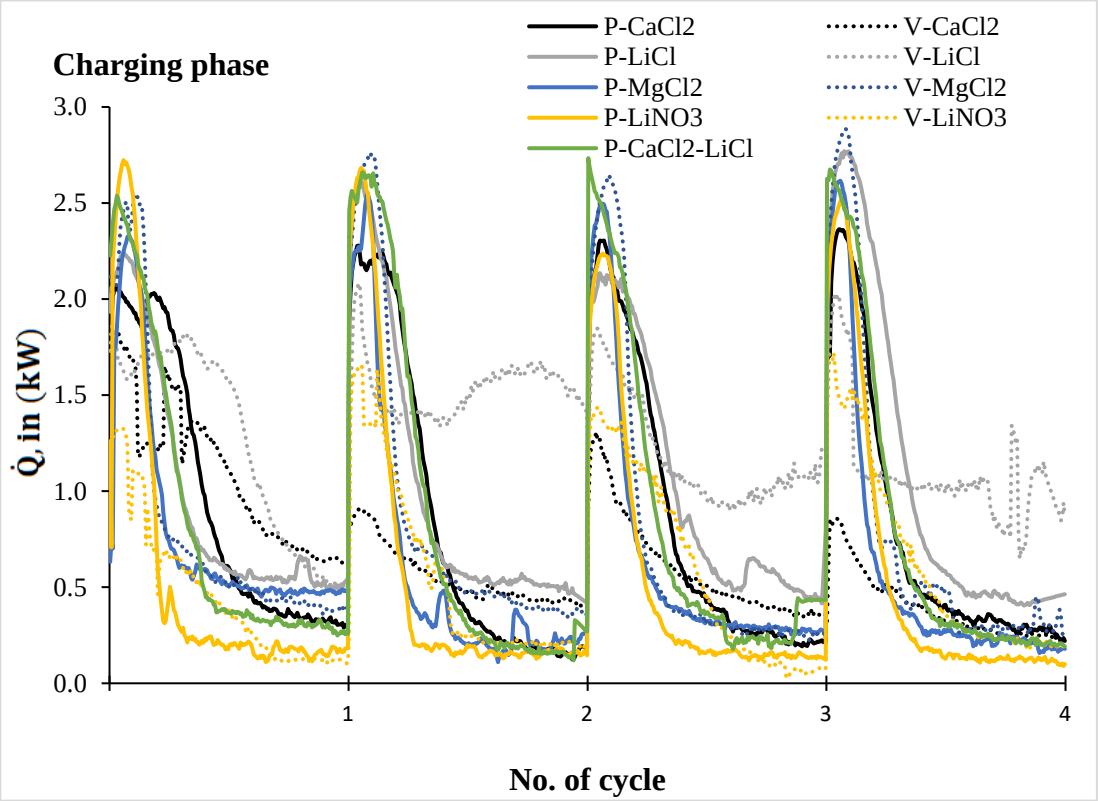

Figure 21: Inlet Energy Rate Variations of Nine Sorption Materials over Four Charging Cycles.

5.2.2 Exergy Analysis

Exergy inlet rate (Ėx, in) variations over charging phases are presented in Figure 22. The charging exergy profiles for the tested materials are lower than the energy profiles. P-$CaCl_2$, P-LiCl and P-$CaCl_2$-LiCl shows a content rate of inlet exergy over the four cycles, and were 0.12, 0.11, 0.11, 0.10 kW, 0.13, 0.12, 0.12, 0.12 kW, and 0.11, 0.11, 0.11, 0.10 kW, respectively. V-$CaCl_2$ showed a decreasing of inlet exergy rates within the cycles, and was 0.14, 0.08, 0.09, and 0.06 kW. In addition, V-LiCl shows the highest rates of inlet exergy in charging cycles, and was 0.16, 0.19, 0.16, and 0.15 kW, respectively. P-$MgCl_2$ shows a lower inlet exergy rate compared to V-$MgCl_2$, and were

0.11, 0.08, 0.08, 0.08kW, and 0.12, 0.12, 0.10, 0.10 kW, respectively. The exergy rate of P-$LiNO_3$ was constant over the four cycles with 0.07 kW. The V-$LiNO_3$ shows exergy rate of 0.06 kW in the first cycle and it was constant in the 2nd, 3rd and 4th cycles with 0.08 kW. In general, the inlet exergy rates in charging processes was found more than 10 times of the outlet exergy rates in discharging, and this is due to the difference between the required T_{ch} and obtained T_{dch}.

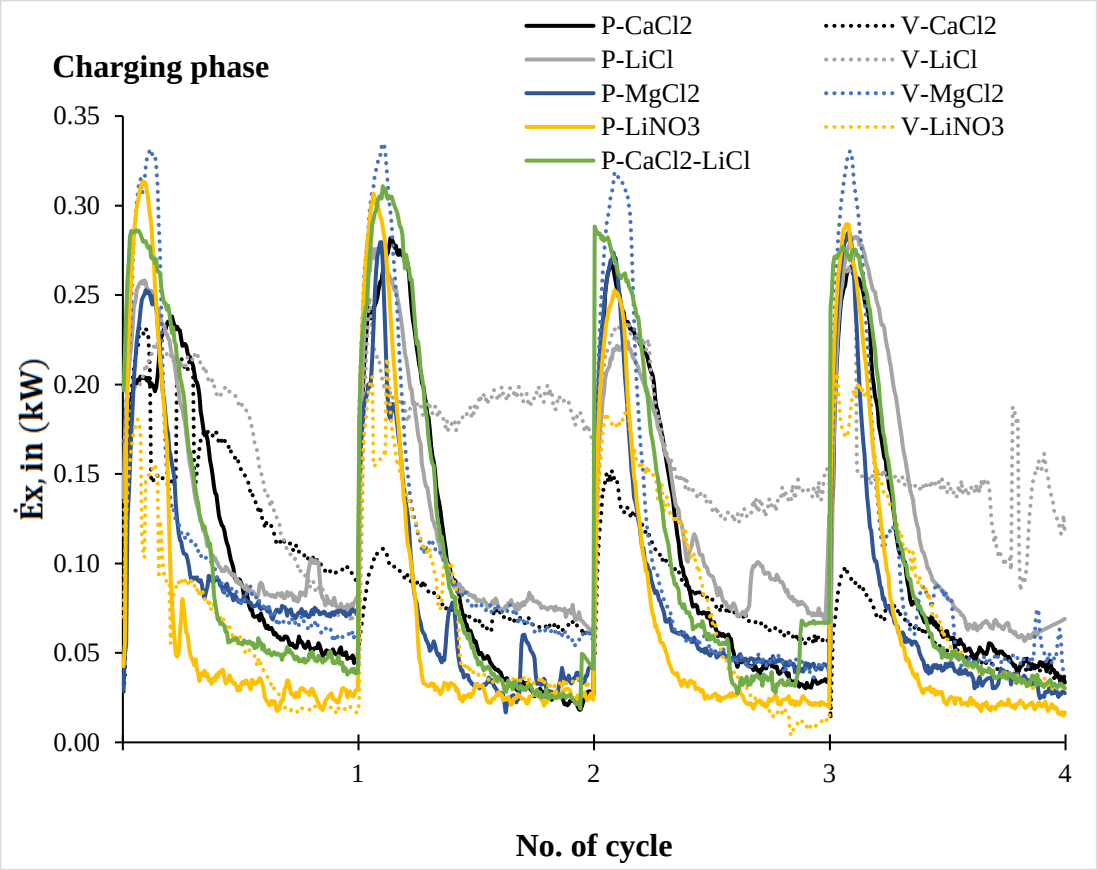

Figure 22: Inlet Exergy Rate Variations of Nine Sorption Materials over Four Charging Cycles.

5.2.3 Moisture Desorption Analysis

View of desorption rates ($\dot{f}_{dsorp}$) during charging cycles of nine sorbents were illustrated in Figure 23. The amount of moisture removed per second of P-$CaCl_2$, P-LiCl and P-$CaCl_2$-LiCl were 0.10, 0.10, 0.11, 0.09 g/s, 0.10, 0.11, 0.07, 0.07 g/s, and

0.10, 0.11, 0.11, 0.11 g/s over four charging cycles respectively. Thus, the above three pumice-salts show almost the same moisture desorption rate, except in the 3rd and 4th cycles of P-LiCl that shows a gradual decrease. In addition, the mixture sorbent of P-$CaCl_2$-LiCl shows a very high and constant desorption rate compared to all other sorbents. V-$CaCl_2$ shows a dramatic decrease of desorption rate from 0.09 g/s in the first cycle to 0.02 g/s in the fourth cycle. V-LiCl shows the highest desorption rate of moisture among all the materials, but it gradually decreased over the charging cycles, and was 0.12, 0.13, 0.10, and 0.08 g/s, respectively. For P-$MgCl_2$ and V-$MgCl_2$, desorption rates were found constant and especially in the second, third and fourth cycles, and was 0.06, 0.07, 0.07, 0.07 g/s, and 0.08, 0.10, 0.10, 0.10 g/s. Moreover, P-$LiNO_3$ and V$LiNO_3$ shows an average of constant desorption rates of 0.05 g/s, and 0.08 g/s, over four successive cycles.

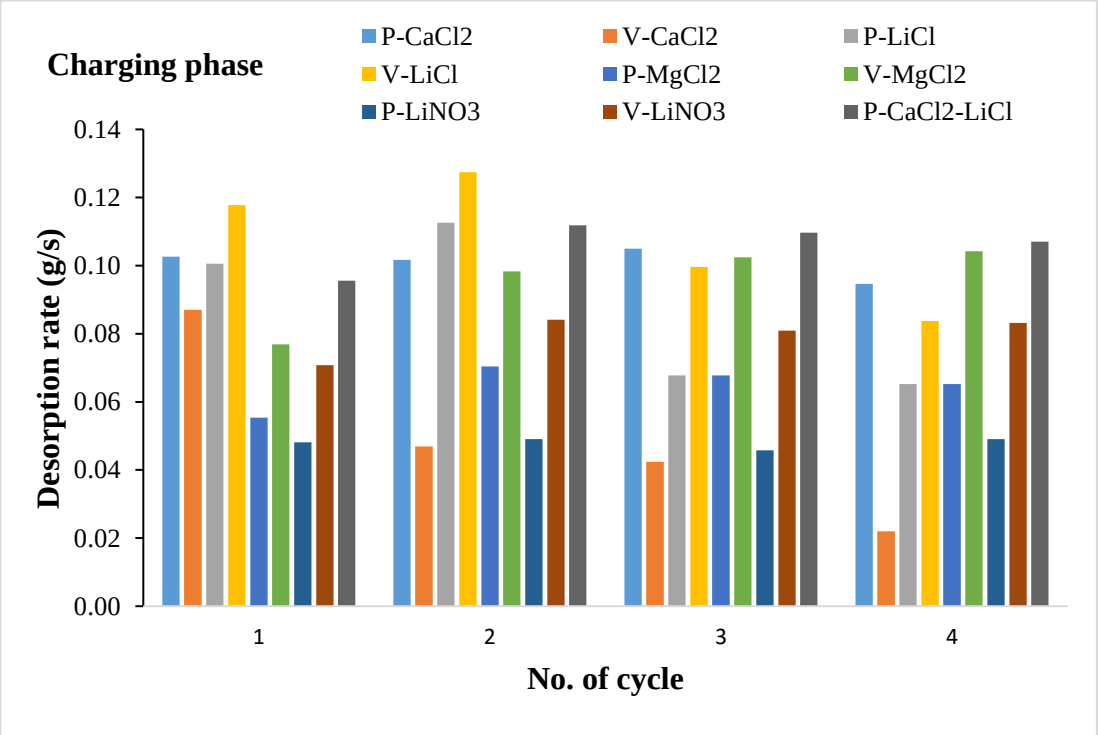

Figure 23: Desorption rate of Nine Sorption Materials over Four Charging Cycles.

The ratio of heat inlet rate per desorption rate ($\dot{Q}/\dot{f}_{dsorp}$) of nine THS materials are presented in Figure 24. The inlet heat per desorption rate of vapor for P-$CaCl_2$, P-LiCl, and P-$CaCl_2$-LiCl were 9, 8, 8, 8 kJ/g, 10, 9, 15, 17 kJ/g, and 9, 8, 8, 7 kJ/g over four charging cycles respectively. Thus, P-$CaCl_2$ and P-LiCl almost showed the same ratio of $\dot{Q}/\dot{f}_{dsorp}$ in all cycles, P-LiCl showed a gradual increase in the ratio, which means that more inlet heat to the sorbent and, as a result, less desorption of moisture in the last two cycles.

As shown the Figure 24, the V-$CaCl_2$ shows an increase in the ratio of heat inlet per desorption rate, and it was 12, 12, 14, and 18 kJ/g. This increase indicates that the high temperature supplied to the reactor's inlet does not affect the material to remove the moisture due to the material's structural degradation. For V-LiCl, the material shows a high and gradually increase of $\dot{Q}/\dot{f}_{dsorp}$ ratio, and was 11, 12, 12, and 13 kJ/g, over the four cycles respectively. Thus, it means that V-LiCl needs high temperature or more duration of time to desorb the vapor.

The $\dot{Q}/\dot{f}_{dsorp}$ of P-$MgCl_2$ and V-$MgCl_2$ over the four cycles was 14, 9, 10, 9 kJ/g, and 11, 9, 7, 7 kJ/g. The P-$LiNO_3$ shows a high and constant ratio of inlet heat per desorption rate in each cycle compared to V-$LiNO_3$, and it was 12, 11, 12, and 11 kJ/g, respectively. Moreover, V- $LiNO_3$ shows the lowest ratio of $\dot{Q}/\dot{f}_{dsorp}$ in all cycles compared to other sorbents, additionally, it was constant in the four cycles with an average of 7 kJ/g.

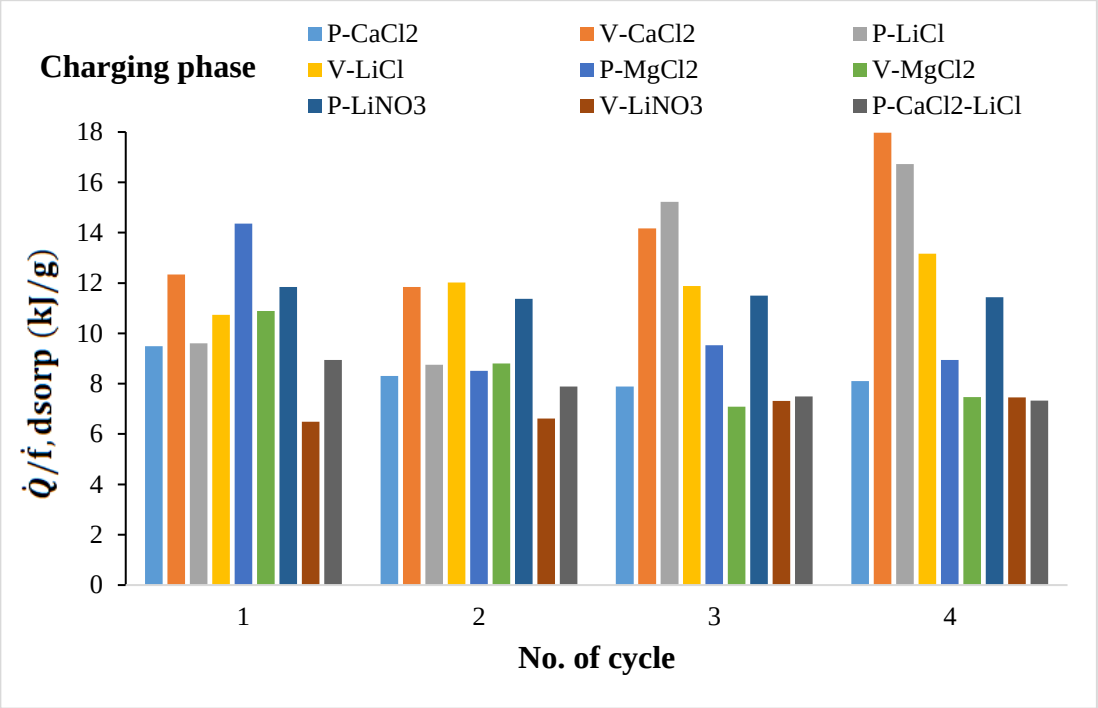

Figure 24: Heat Inlet Rate per Desorption Rate of Nine Sorption Materials over Four Charging Cycles.

The ratio of exergy inlet rate per desorption rate ($\dot{E}x/\dot{f}_{dsorp}$) profiles of nine sorbents in charging processes are presented in Figure 25. P-$CaCl_2$ and P-$CaCl_2$-LiCl show a lower exergy ratio per desorption rate among all sorbents, and were 1.16, 1.06, 1.01, 1.05 kJ/g, and 1.19, 1.01, 0.99. 94 kJ/g over the four cycles. V-$CaCl_2$ showed an increase within cycles and was 1.63, 1.62, 2.05, and 2.59 kJ/g. In addition, the exergy rate per desorption rate of V-LiCl increased over the cycles and was 1.33, 1.48, 1.59, and 1.79 kJ/g, respectively. For P-$MgCl_2$ and V-$MgCl_2$, the ratio of exergy inlet rate per desorption rate was decreased gradually over the four cycles, and was 1.91, 1.08, 1.24, 1.15 kJ/g, and 1.54, 1.21, 0.96, 1.00 kJ/g. The P-$LiNO_3$ shows a high and constant ratio of inlet exergy per desorption rate in each cycle compared to V- $LiNO_3$, and it was 1.56, 1.51, 1.44, and 1.49 kJ/g, respectively. Moreover, V- $LiNO_3$ shows a low ratio of $\dot{E}x/\dot{f}_{dsorp}$ in all cycles compared to other sorbents; additionally, it was almost constant in the four cycles with an average of 0.95 kJ/g.

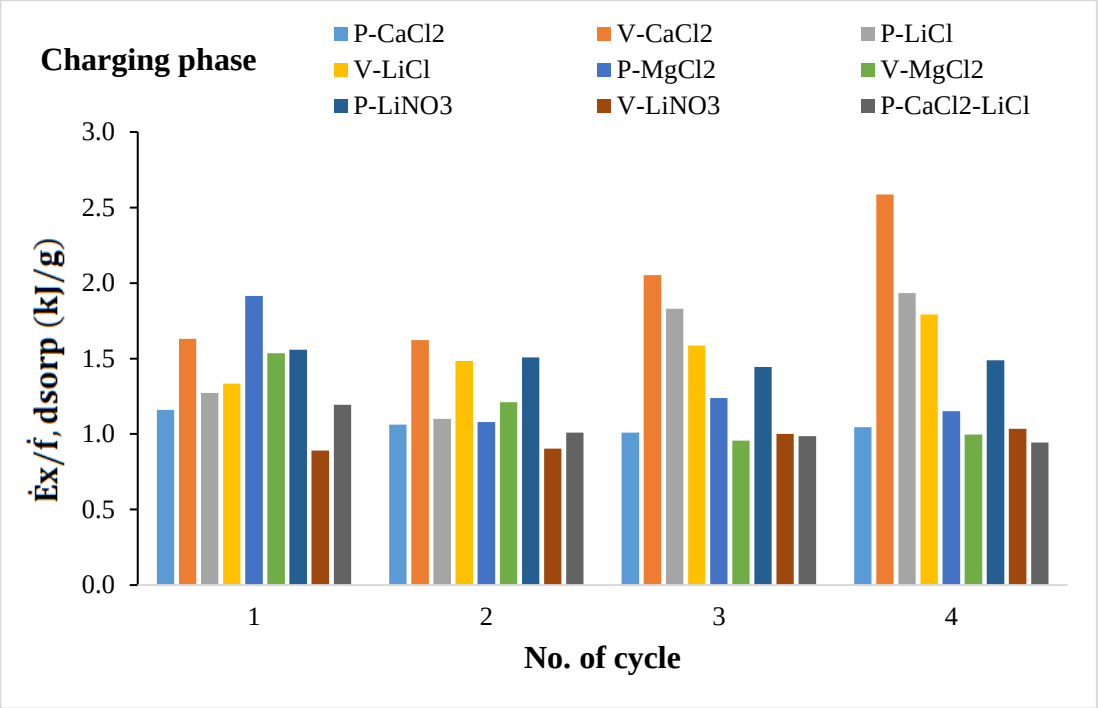

Figure 25: Exergy Inlet Rate per Desorption Rate of Nine Sorption Materials over Four Charging Cycles

5.3 Overall Performance Analysis

Initial and final views of the sorption materials before and after testing were presented in Figure 26 and 27, respectively. From the figures, no degeneration occurred to the sorbents' structure after the discharging and charging cycles, except V-$CaCl_2$, that shows a structural degradation after the 3rd and 4th cycles. Thus, the tested materials show physical stability when they are not over saturated. Additionally, when the tested materials are over-saturated, structural deformation may occur, exactly the same as V-$CaCl_2$ that was over saturated and its structural deformed and became mushy, which is not a desired property. The host matrix of vermiculite is a very soft material, the amount of moisture absorbed during discharging cycles it should be taken into consideration.

Figure 26: Initial View of the Sorption Materials Before Testing: (a) P-$CaCl_2$, (b) V-$CaCl_2$, (c) P-LiCl, (d) V-LiCl, (e) P-$MgCl_2$ (f) V-$MgCl_2$, (g) P-$LiNO_3$, (h) V-$LiNO_3$, and (i) P-$CaCl_2$- LiCl.

As shown in Figure 27, the color of most of the sorption materials shows a change between the initial and final views. The final view of P-$CaCl_2$ looked brighter (almost same as initial view) because the material was not over saturated over repeating cycles. In P-LiCl and P-$CaCl_2$-LiCl, the materials look the same after and before testing because more than 90 % of moisture was removed over the four charging cycles. V-LiCl was over saturated, and that is why it looks darker. P-$MgCl_2$, V-$MgCl_2$, P-$LiNO_3$, and V-$LiNO_3$ show different colors before and after the experimental tests.

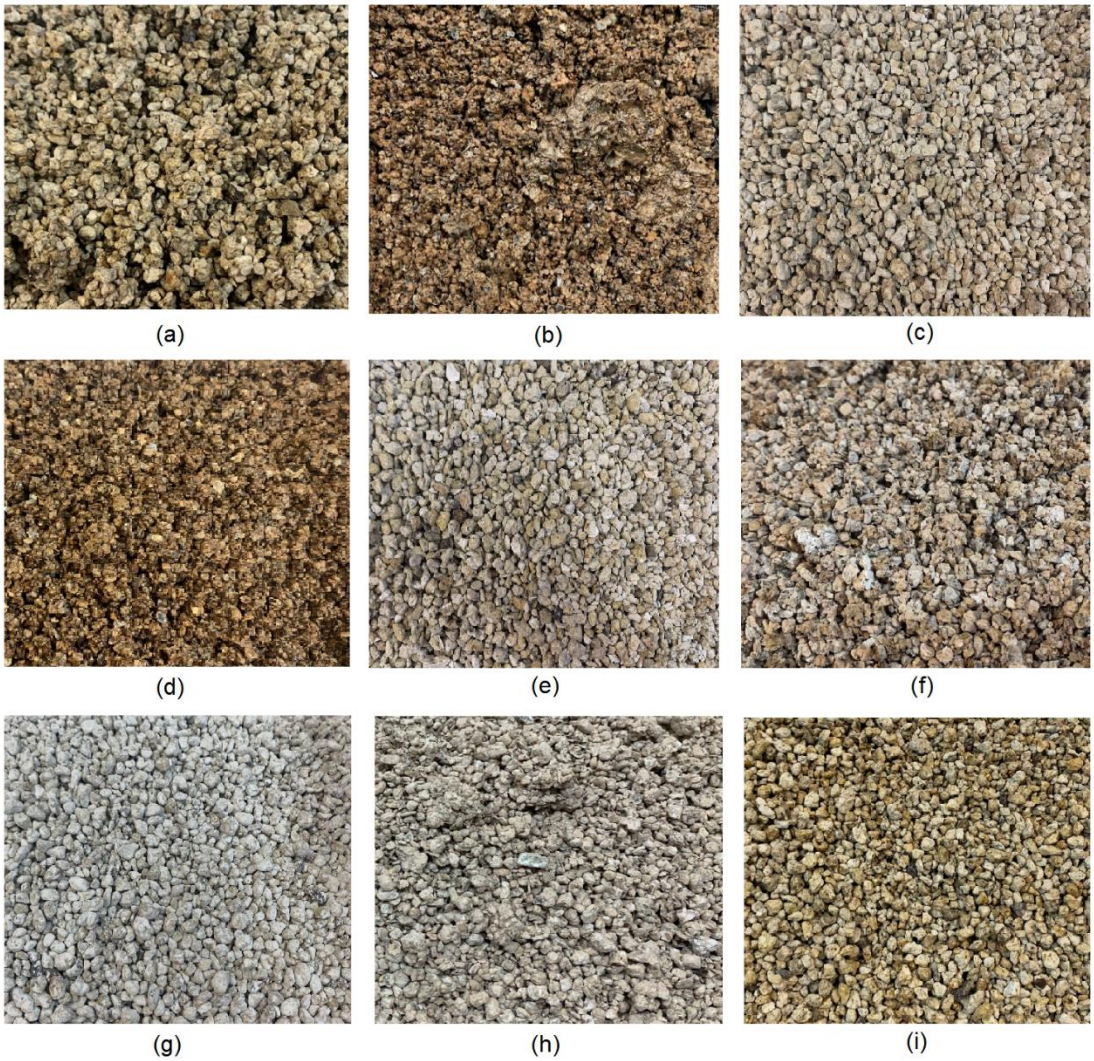

Figure 27: Final View of the Sorption Materials After Testing: (a) P-$CaCl_2$, (b) V-$CaCl_2$, (c) P-LiCl, (d) V-LiCl, (e) P-$MgCl_2$ (f) V-$MgCl_2$, (g) P-$LiNO_3$, (h) V-$LiNO_3$, and (i) P-$CaCl_2$- LiCl.

In Figure 28, the energetic efficiencies (η_I) of nine sorbents after discharging/charging processes are presented. The energetic efficiency of P-$CaCl_2$ was almost steady and high, and was 71, 63, 63, and 69 % over four successive cycles. P-LiCl shows a high energetic efficiency in the first cycle and it was 86 %, and then it drops to 53 % in the last cycle. In addition, P-$CaCl_2$-LiCl shows a dramatically drop of energetic efficiency from the 1st to 2nd cycle, and then it becomes steadier in the 2nd, 3rd, and 4th cycles, and was found 90, 65, 64, and 64 %, respectively. V-$CaCl_2$ shows a high energetic efficiency in the 1st and 2nd cycles with an average of 81 %, and then it dramatically

drops in 3rd and 4th cycles with an average of 25 %. For V-LiCl, the first law efficiency was high but it decreases gradually over the four cycles and this due to insufficient of charging period, and it was 90, 72, 72, 62 %, respectively. The energetic efficiency of P-$MgCl_2$ was 60, 58, 55, and 54 %, and of V-$MgCl_2$ was 82, 56, 63, and 53 %. Moreover, the energetic efficiencies of P-$LiNO_3$ and V-$LiNO_3$ in each cycle increased and were, 39, 50, 59, 62 %, and 63, 54, 68, 77 %, respectively.

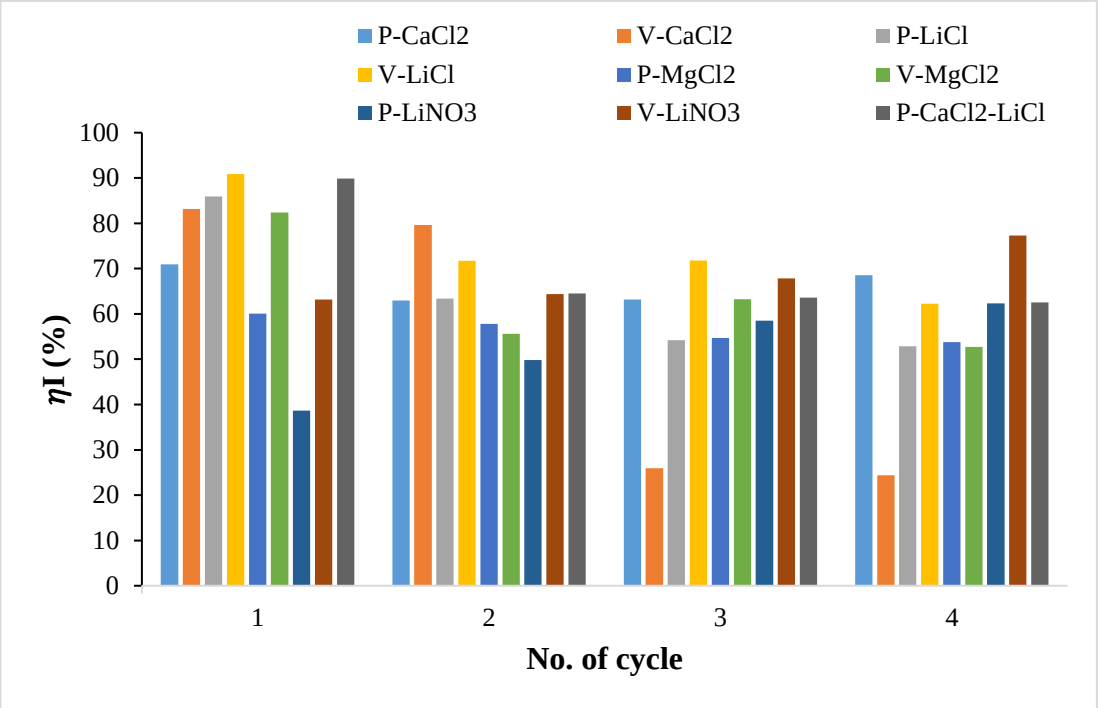

Figure 28: Energetic Efficiencies of Nine Sorption Materials.

After discharging and charging phases, the exergetic efficiencies (η_{II}) of nine sorbents are shown in Figure 29. In the first cycle, the exergetic efficiency of most of the materials was higher than the 2nd, 3rd, and 4th cycles, except P-$LiNO_3$ and V-$LiNO_3$, which shows a gradual increase of efficiency. The exergetic efficiencies of P-$CaCl_2$, P-LiCl, and P-$CaCl_2$-LiCl over the four cycles were 7.0, 3.6, 3.5, 4.1 %, 11.8, 6.3, 5.5, 4.7 %, and 11.1, 6.0, 5.3, 5.5 %, respectively. V-$CaCl_2$ showed a considerable drop in the exergetic efficiency and was 15.4, 7.1, 0.1, and 0.1 %. In V-LiCl, the exergetic

efficiency was very high in the 1st, 2nd, and 3rd cycles, and was 17.6, 12.1, 10.0, and 5.6, respectively. The exergetic efficiencies of P-$MgCl_2$ and V-$MgCl_2$ were 3.3, 1.6, 1.8, 1.1 %, and 9.4, 2.3, 3.9, 2.2 %, over four cycles respectively. Both P-$LiNO_3$ and V-$LiNO_3$, shows a gradual increase of exergetic efficiencies, and were 0.7, 2.0, 2.6, 5.6 %, and 3.2, 4.5, 5.1, 5.9 %, respectively.

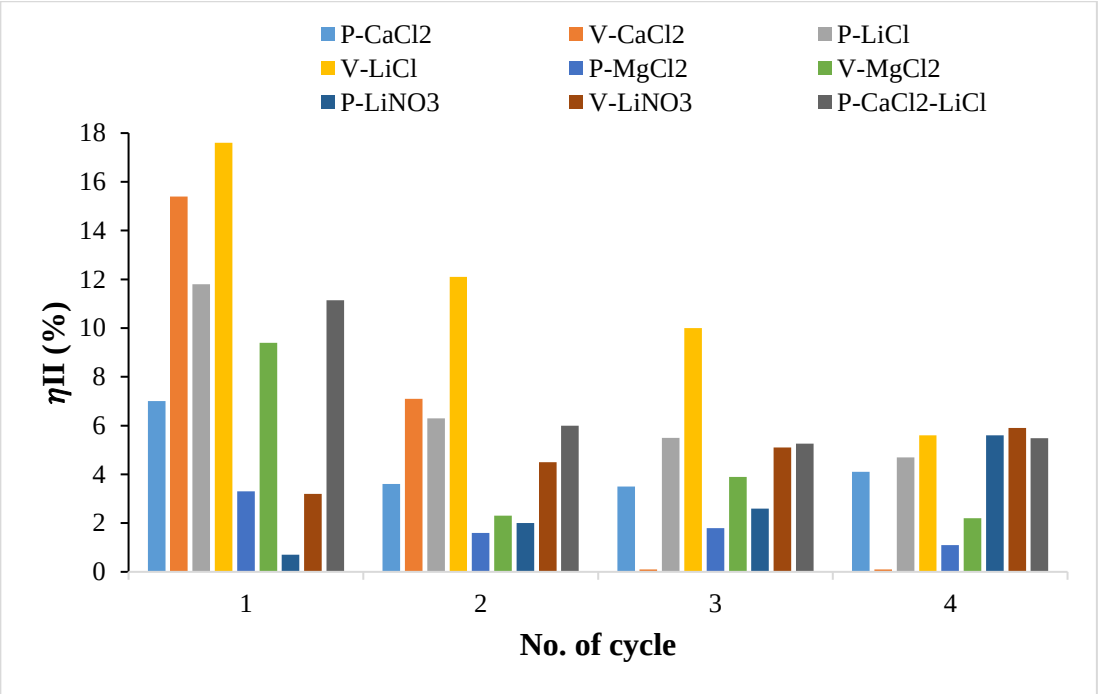

Figure 29: Exergetic Efficiencies of Nine Sorption Materials.

The hygro-cyclic efficiencies (η_{hyg}) of nine tested materials are presented in Figure 30. The ratio of absorption/ desorption characteristics is referred to as hygro-cyclic efficiency, and it is used to provide more accurate comparisons between the sorption materials. The hygro-cyclic efficiency of P-$CaCl_2$, P-LiCl, and P-$CaCl_2$-LiCl over the four cycles were 77, 80, 85, 86 %, 74, 85, 92, 93 %, and 73, 85, 93, 98 %, respectively. Therefore, P-$CaCl_2$-LiCl shows the highest hygro-cyclic efficiency compared to all other materials, which means the material was almost totally adsorbed the moisture to be dried. V-$CaCl_2$ showed a drop in efficiency and was 53, 24, 25, and 16 %. For V-

LiCl, the material showed a gradual decrease in the hygro-cyclic efficiency and was 56, 55, 44, and 43 %, which means the material could not remove vapor over cycles; the used regeneration temperature is low because of the short charging duration. The hygro-cyclic efficiencies of P-$MgCl_2$ and V-$MgCl_2$ were 70, 72, 68, 67 %, and 70, 73, 77, 78 %, over four cycles respectively. Both P-$LiNO_3$ and V-$LiNO_3$ showed a slight increase in hygro-cyclic efficiency and was 85, 86, 87, 88 %, and 85, 87, 88, 89 %, respectively.

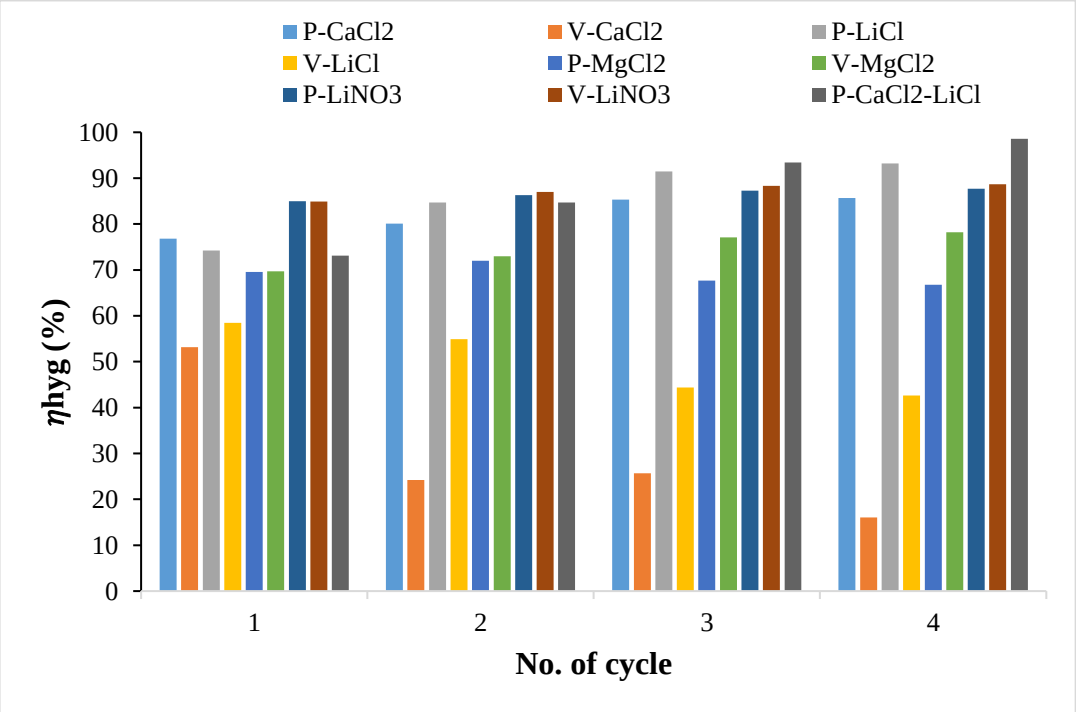

Figure 30: Hygro-cyclic Efficiencies of Nine Sorption Materials.

Figure 31 shows the measured mass fluctuations of the nine sorbents following discharging and charging phases. Increased and decreased trend of mass fluctuations in the figure represent the quantity of moisture absorbed and desorbed, respectively. P-$CaCl_2$, P-LiCl, and P-$CaCl_2$-LiCl show a decrease in the last cycles, meaning more moisture was removed. V-$CaCl_2$ shows a failure in the last cycles, with no absorption and desorption. In V-LiCl, the material shows less mass changes. Each material of P-

$MgCl_2$, V-$MgCl_2$, P-$LiNO_3$, and V-$LiNO_3$ shows slight mass changes over discharging and charging cycles.

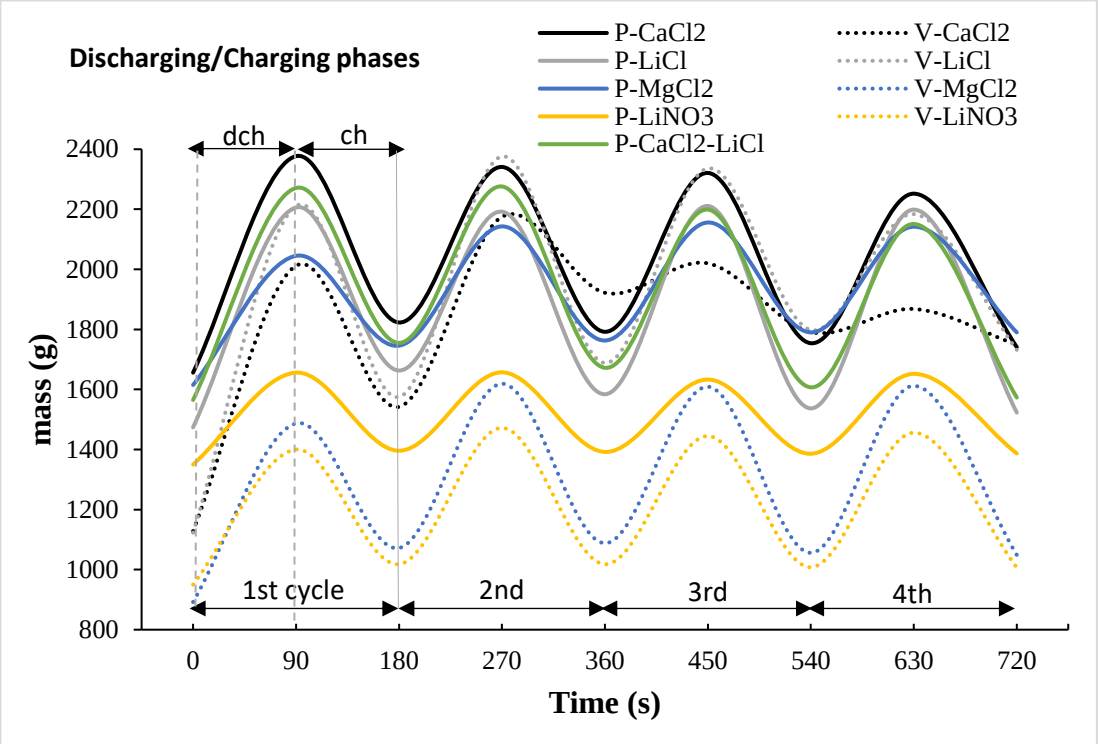

Figure 31: Mass Variations of Nine Sorption Materials over Four Discharging/Charging Cycles.

The overall summary results of the nine tested sorbents over four discharging and charging processes are shown in Table 3 and 4, respectively. The testing of each sorbent began after it had thoroughly dried in an electrical furnace at a temperature of 150°C; discharging and charging cycles tests were applied for four successive cycles. The overall summery of energetic (η_I), exergetic (η_{II}) and hygro-cyclic (η_{hyg}) efficiencies for the nine tested sorbents over four cycles are presented in Table 5. The overall mass changes of sorbents after discharging/charging phases are shown in Table 6.

Table 3: Overall Summary of Discharging Performance of Nine Tested Sorption Materials over Four Cycles.

Material	Cycle	T_{out} ℃	ΔT_{avg} ℃	ΔRH_{avg} %	v m/s	$\dot{Q}$ kW	E_{cum} kWh	$\dot{E}x$ kW	Ex_{cum} kWh	$\dot{f}_{sorp}$ g/s	$\dot{Q}/\dot{f}_{sorp}$ kJ/g	$\dot{E}x/\dot{f}_{sorp}$ kJ/g	E_d kWh/m^3	V m^3
P-$CaCl_2$	1	33.5	11.0	54	3.1	0.690	1.036	0.008	0.012	0.13	5.17	0.06	296	0.0035
	2	31.6	8.1	42	3.2	0.532	0.797	0.004	0.006	0.10	5.55	0.04	228	0.0035
	3	30.9	8.8	47	2.9	0.523	0.784	0.004	0.006	0.10	5.34	0.04	224	0.0035
	4	30.7	8.3	41	3.1	0.526	0.788	0.004	0.006	0.09	5.70	0.04	225	0.0035
V-$CaCl_2$	1	40.0	19.1	73	2.3	0.894	1.340	0.022	0.033	0.16	5.46	0.13	383	0.0035
	2	33.8	11.4	60	1.9	0.442	0.663	0.005	0.008	0.12	3.77	0.04	189	0.0035
	3	24.9	2.6	24	2.9	0.156	0.234	0.000	0.000	0.02	8.60	0.00	67	0.0035
	4	25.3	3.0	24	1.6	0.097	0.145	0.000	0.000	0.01	6.80	0.00	41	0.0035
P-LiCl	1	36.9	14.6	66	2.8	0.830	1.245	0.015	0.023	0.14	6.12	0.11	356	0.0035
	2	33.3	9.9	48	3.1	0.624	0.936	0.008	0.012	0.10	6.37	0.08	267	0.0035
	3	32.6	9.8	50	2.8	0.559	0.838	0.007	0.010	0.12	4.81	0.06	240	0.0035
	4	34.2	9.7	49	2.9	0.576	0.864	0.006	0.009	0.12	4.70	0.05	247	0.0035
V-LiCl	1	42.4	20.2	71	2.8	1.149	1.724	0.028	0.041	0.20	5.70	0.14	492	0.0035
	2	42.0	17.9	66	3.0	1.098	1.647	0.023	0.034	0.15	7.40	0.16	471	0.0035
	3	37.4	14.9	69	2.8	0.850	1.275	0.016	0.024	0.12	7.08	0.13	364	0.0035
	4	34.5	11.2	57	3.0	0.686	1.029	0.008	0.013	0.07	9.60	0.11	294	0.0035
P-$MgCl_2$	1	30.7	7.8	46	3.0	0.478	0.717	0.003	0.005	0.08	6.00	0.04	205	0.0035
	2	27.3	5.3	37	3.2	0.346	0.519	0.001	0.002	0.07	4.71	0.01	148	0.0035
	3	27.7	5.8	40	3.0	0.353	0.530	0.002	0.002	0.07	4.85	0.03	151	0.0035
	4	26.7	5.1	36	3.0	0.313	0.470	0.001	0.001	0.07	4.80	0.02	134	0.0035
V-$MgCl_2$	1	33.6	13.1	62	2.6	0.690	1.034	0.011	0.017	0.11	6.26	0.10	296	0.0035
	2	27.7	7.9	49	3.0	0.482	0.723	0.003	0.004	0.10	4.76	0.03	206	0.0035
	3	27.0	8.0	51	2.8	0.459	0.689	0.004	0.006	0.10	4.76	0.04	197	0.0035
	4	26.6	6.7	44	3.0	0.410	0.615	0.002	0.003	0.10	3.98	0.02	176	0.0035
P-$LiNO_3$	1	23.1	4.5	37	2.4	0.220	0.331	0.001	0.001	0.06	3.88	0.02	94	0.0035
	2	24.7	4.9	36	2.8	0.278	0.417	0.001	0.002	0.05	5.75	0.02	119	0.0035
	3	27.4	6.0	39	2.5	0.308	0.462	0.002	0.003	0.04	6.90	0.04	132	0.0035
	4	27.6	6.9	45	2.5	0.350	0.525	0.004	0.006	0.05	7.11	0.08	150	0.0035

Table 3 cont.

V-$LiNO_3$	1	28.4	7.9	51	1.8	0.290	0.435	0.002	0.003	0.08	3.48	0.02	124	0.0035
	2	30.4	9.7	59	1.8	0.358	0.537	0.003	0.005	0.08	4.26	0.04	153	0.0035
	3	28.5	9.8	61	2.0	0.401	0.602	0.004	0.006	0.08	5.07	0.05	172	0.0035
	4	31.1	10.7	63	2.2	0.479	0.719	0.005	0.008	0.08	5.77	0.06	205	0.0035
P-$CaCl_2$-LiCl	1	33.6	12.6	56	3.0	0.768	1.152	0.013	0.019	0.13	5.87	0.10	329	0.0035
	2	30.3	8.7	45	3.2	0.569	0.853	0.007	0.010	0.10	5.90	0.07	244	0.0035
	3	30.0	8.8	46	2.9	0.522	0.783	0.006	0.008	0.10	5.35	0.06	224	0.0035
	4	29.8	8.0	43	3.0	0.490	0.735	0.006	0.008	0.10	4.86	0.06	210	0.0035

Table 4: Overall Summary of Charging Performance of Nine Tested Sorption Materials over Four Cycles.

Material	Cycle	T_{out} ℃	ΔT_{avg} ℃	ΔRH_{avg} %	v m/s	$\dot{Q}$ kW	E_{cum} kWh	$\dot{E}x$ kW	Ex_{cum} kWh	$\dot{f}_{dsorp}$ g/s	$\dot{Q}/\dot{f}_{dsorp}$ kJ/g	$\dot{E}x/\dot{f}_{dsorp}$ kJ/g	V m^3
P-$CaCl_2$	1	65.5	16.2	9.9	3.4	0.973	1.460	0.119	0.179	0.10	9.48	1.16	0.0035
	2	68.6	13.3	8.5	3.6	0.844	1.267	0.108	0.162	0.10	8.30	1.06	0.0035
	3	68.7	13.1	8.4	3.6	0.828	1.241	0.106	0.160	0.11	7.89	1.01	0.0035
	4	69.8	11.9	6.8	3.7	0.767	1.150	0.099	0.149	0.09	8.11	1.05	0.0035
V-$CaCl_2$	1	58.6	23.4	5.5	2.6	1.074	1.611	0.142	0.213	0.09	12.34	1.63	0.0035
	2	67.0	15.0	6.3	2.1	0.555	0.833	0.076	0.114	0.05	11.85	1.62	0.0035
	3	72.0	9.8	4.1	3.5	0.601	0.901	0.087	0.131	0.04	14.17	2.05	0.0035
	4	72.5	9.4	3.9	2.4	0.396	0.595	0.057	0.085	0.02	17.97	2.59	0.0035
P-LiCl	1	66.6	15.6	6.2	3.5	0.966	1.448	0.128	0.192	0.10	9.61	1.27	0.0035
	2	66.7	15.1	7.2	3.7	0.985	1.477	0.124	0.186	0.11	8.75	1.10	0.0035
	3	64.7	17.7	10.3	3.3	1.032	1.548	0.124	0.186	0.07	15.23	1.83	0.0035
	4	64.6	17.8	9.4	3.5	1.090	1.634	0.126	0.190	0.07	16.72	1.93	0.0035
V-LiCl	1	62.7	19.9	6.0	3.6	1.265	1.897	0.157	0.235	0.12	10.74	1.33	0.0035
	2	58.9	23.5	7.8	3.7	1.531	2.297	0.189	0.283	0.13	12.02	1.48	0.0035
	3	61.8	20.4	7.6	3.3	1.184	1.776	0.158	0.237	0.10	11.88	1.59	0.0035
	4	65.1	17.5	5.8	3.6	1.102	1.653	0.150	0.224	0.08	13.17	1.79	0.0035
P-$MgCl_2$	1	69.6	12.5	6.7	3.6	0.795	1.193	0.106	0.159	0.06	14.36	1.91	0.0035
	2	72.6	9.2	7.8	3.2	0.599	0.898	0.076	0.114	0.07	8.51	1.08	0.0035
	3	71.1	10.8	8.2	3.4	0.646	0.969	0.084	0.126	0.07	9.53	1.24	0.0035
	4	72.6	9.5	7.4	3.5	0.583	0.874	0.075	0.113	0.07	8.94	1.15	0.0035
V-$MgCl_2$	1	69.1	12.8	6.2	3.7	0.837	1.255	0.118	0.176	0.08	10.89	1.54	0.0035
	2	68.7	13.3	8.3	3.7	0.866	1.300	0.119	0.178	0.10	8.81	1.21	0.0035
	3	69.3	12.5	9.5	3.3	0.726	1.089	0.098	0.148	0.10	7.09	0.96	0.0035
	4	70.0	12.4	9.3	3.6	0.778	1.167	0.104	0.156	0.10	7.46	1.00	0.0035
P-$LiNO_3$	1	72.4	9.2	7.8	3.5	0.570	0.855	0.075	0.112	0.05	11.84	1.56	0.0035
	2	72.5	9.1	7.9	3.5	0.558	0.837	0.074	0.111	0.05	11.37	1.51	0.0035
	3	71.9	10.0	8.6	3.0	0.526	0.789	0.066	0.099	0.05	11.50	1.44	0.0035
	4	71.7	9.7	8.4	3.3	0.561	0.842	0.073	0.110	0.05	11.43	1.49	0.0035

Table 4 cont.

V-$LiNO_3$	1	68.4	13.0	6.2	2.0	0.459	0.688	0.063	0.095	0.07	6.49	0.89	0.0035
	2	69.5	12.6	6.9	2.5	0.556	0.833	0.076	0.115	0.08	6.61	0.90	0.0035
	3	66.7	14.6	8.3	2.3	0.592	0.888	0.081	0.122	0.08	7.32	1.00	0.0035
	4	68.5	13.6	6.5	2.6	0.620	0.930	0.086	0.129	0.08	7.46	1.03	0.0035
P-$CaCl_2$-LiCl	1	68.2	13.8	8.6	3.5	0.854	1.281	0.114	0.171	0.10	8.94	1.19	0.0035
	2	68.6	12.9	10.8	3.9	0.882	1.323	0.113	0.169	0.11	7.89	1.01	0.0035
	3	69.3	13.3	9.6	3.5	0.821	1.231	0.108	0.162	0.11	7.49	0.99	0.0035
	4	70.1	12.4	9.3	3.6	0.784	1.176	0.101	0.151	0.11	7.32	0.94	0.0035

Table 5: Overall Summary of Energetic, Exergetic and Hygro-cyclic Efficiencies of Nine Tested Sorption Materials over Four Cycles.

Material	Cycle	η_I (%) ±5.1%	η_{II} (%) ±6.8%	η_{hyg} (%)
P-$CaCl_2$	1	71.0	7.0	76.8
	2	63.0	3.6	80.1
	3	63.2	3.5	85.3
	4	68.5	4.1	85.7
V-$CaCl_2$	1	83.2	15.4	53.2
	2	79.6	7.1	24.2
	3	26.0	0.1	25.7
	4	24.4	0.1	16.1
P- LiCl	1	85.9	11.8	74.2
	2	63.4	6.3	84.7
	3	54.2	5.5	91.5
	4	52.9	4.7	93.2
V-LiCl	1	90.9	17.6	58.5
	2	71.7	12.1	54.9
	3	71.8	10.0	44.4
	4	62.2	5.6	42.6
P-$MgCl_2$	1	60.1	3.3	69.5
	2	57.8	1.6	72.0
	3	54.7	1.8	67.7
	4	53.8	1.1	66.8
V-$MgCl_2$	1	82.4	9.4	69.7
	2	55.6	2.3	73.0
	3	63.2	3.9	77.1
	4	52.7	2.2	78.2
P-$LiNO_3$	1	38.7	0.7	85.0
	2	49.8	2.0	86.3
	3	58.5	2.6	87.3
	4	62.3	5.6	87.7
V-$LiNO_3$	1	63.1	3.2	84.9
	2	64.4	4.5	87.0
	3	67.8	5.1	88.3
	4	77.3	5.9	88.7
P-$CaCl_2$-LiCl	1	89.9	11.1	73.1
	2	64.5	6.0	84.7
	3	63.6	5.3	93.4
	4	62.5	5.5	98.6

Table 6: Overall Summary of Mass Changes of Nine Tested Sorption Materials over Four Cycles.

Material	Cycle	m_{dry} g	m_{dch} g	m_{ch} g	$m_{vapor,sorp}$ g	$m_{vapor,dsorp}$ g
P-$CaCl_2$	1	1656	2377	1823	721	554
	2		2341	1792	518	549
	3		2321	1754	529	567
	4		2252	1741	498	511
V-$CaCl_2$	1	1128	2012	1542	884	470
	2		2175	1922	633	253
	3		2020	1791	98	229
	4		1868	1749	77	119
P- LiCl	1	1474	2206	1663	732	543
	2		2192	1584	529	608
	3		2211	1537	627	366
	4		2199	1523	662	352
V-LiCl	1	1123	2211	1575	1088	636
	2		2376	1688	801	688
	3		2336	1798	648	538
	4		2184	1732	386	452
P-$MgCl_2$	1	1615	2045	1746	430	299
	2		2143	1763	397	380
	3		2156	1790	393	366
	4		2142	1790	352	352
V-$MgCl_2$	1	892	1487	1072	595	415
	2		1619	1088	547	531
	3		1609	1056	521	553
	4		1612	1049	556	563
P-$LiNO_3$	1	1350	1656	1396	306	260
	2		1657	1392	261	265
	3		1633	1386	241	247
	4		1652	1387	266	265
V-$LiNO_3$	1	950	1400	1018	450	382
	2		1472	1018	454	454
	3		1445	1008	427	437
	4		1456	1007	448	449
P-$CaCl_2$-LiCl	1	1565	2271	1755	706	516
	2		2276	1672	521	604
	3		2199	1607	527	592
	4		2151	1573	544	578

Chapter 6

CONCLUSION AND FUTURE WORKS

6.1 Conclusion

In this experimental study, nine different THS materials were synthesized using pumice and vermiculite as the host matrices, and $CaCl_2$, LiCl, $MgCl_2$, $LiNO_3$ as the sorbents, and then they were experimentally investigated in an open THS system. One of the tested materials was a mixture of two hygroscopic salts ($CaCl_2$+LiCl) with a ratio of 1:1 (mass basis) impregnated into pumice, and which was synthesized based on the best results achieved from the experimental test of mono-salt composites. In addition, all the sorption materials using pumice as a host matrix and hygroscopic salts as sorbents were novel in this study, except P-$CaCl_2$, which was recently studied in the literature. Whereas, the other hygroscopic salts impregnated into the vermiculite were studied widely in the literature and they were tested again here and compared with all novel sorbents. Within this study, a comparative energetic, exergetic and hygro-cyclic analysis and performance comparison between P-$CaCl_2$, V-$CaCl_2$, P-LiCl, V-LiCl, P-$MgCl_2$, V-$MgCl_2$, P-$LiNO_3$, V-$LiNO_3$, and P-$CaCl_2$-LiCl has been performed. Accordingly, the main conclusions of the study results are as follows:

- Discharging cycles were carried out over 1.5 h with operating states conditions of; $T_{in} = 19 - 23$ ℃, RH=80-85 %, with different measured mass flow rates for every cycle and material. Within four successive cycles, the ΔT_{avg} of P-$CaCl_2$, V-$CaCl_2$, P-LiCl, V-LiCl, P-$MgCl_2$, V-$MgCl_2$, P-$LiNO_3$, V-$LiNO_3$, and P-$CaCl_2$-LiCl was obtained between 11→8 °C, 19→3 °C, 15→10 °C, 20→11

°C, 8→5 °C, 13→7 °C, 5→7 °C, 8→11 °C and 13→8 °C, respectively. Similarly, for the same order of the sorption materials, E_d was varied in the range of 296→225, 383→41, 356→247, 493→294, 205→134, 296→176, 95→150, 124→205, and 329→210 kWh/m^3. Accordingly, the ΔT_{avg} and E_d of most of the sorbents showed a drop from the first to second cycles, and then they becames structural stable in the second, third, and fourth cycles, except for P-$LiNO_3$ and V-$LiNO_3$ that showed a gradual increase due to some moisture absorbed while storing them in containers prior the test. In addition, V-$CaCl_2$ shows a considerable decrease after the first cycle of all the energetic, exergetic performances due to the high amount of moisture absorbed during the first discharging cycle, so the material structural degradation occurs. V-LiCl showed very high performances in the initial cycle, but it showed a gradual decrease in all performances over the four cycles due to low desorption of moisture in the charging phase.

- In the charging cycles, the experimental tests were performed over 1.5 h with operating states of; $T_{in} = 80 - 85\ °C$ and with different measured $\dot{m}_{ch}$ for every cycle and material. Over the four cycles, V-$CaCl_2$ and V-LiCl showed poor desorption kinetics when they were compared with all other sorbents. Whereas the η_{hyg} for P-$CaCl_2$, P-LiCl, P-$MgCl_2$, V-$MgCl_2$, P-$LiNO_3$, V-$LiNO_3$ and P-$CaCl_2$-LiCl, was obtained between 77→86 %, 74→93 %, 70→67 %, 70→78 %, 85→88 %, 85→89 %, and 73→99 %, respectively.

Within the performed study, P-$CaCl_2$, P-LiCl, V-LiCl, and P-$CaCl_2$-LiCl showed an average energy storage density >200 kWh/m^3 and presents superior performances compared with the previously developed sorption materials, whereas

P-$MgCl_2$ and V-$MgCl_2$ showed E_d >130 kWh/m^3. Additionally, P-$LiNO_3$ and V-$LiNO_3$ showed a gradual increase in terms of energy density, due to the high desorption kinetic of the materials.

The obtained results from the tested sorption materials of P-CaCl2, V-CaCl2, V-LiCl, V-MgCl2, and V-LiNO3 shows a higher energy density compared to the earlier studies with the same sorption materials in the literature. For example, the energy density of P-$CaCl_2$ was found 175 kWh/m^3 in the literature [8], while in this study, it was found 225 kWh/m^3. In addition, V-$CaCl_2$ showed a very promising performance initially compared to the literature, but due to the over-saturation of the sorbent over repeating cycles, the material is damaged.

The developed P-$CaCl_2$, P-LiCl, and P-$CaCl_2$-LiCl composites showed a high structural, thermal, desorption kinetics, and performance stability over the second, third and fourth cycles. Pumice provides more promising structural stability when compared with the spongy structure of vermiculite. In addition, pumice reduces air pressure drop, allowing more consistent mass and heat movement throughout the sorption bed. All sorbents showed good structural, thermal, desorption kinetics, and performance stability, except V-$CaCl_2$, which decreased dramatically, and V-LiCl, which decreased gradually in all performances over the four cycles.

6.2 Future Works

According to the experimental results, new improvements could be made to the THS system to ensure that the system is ready to be used with high performance and different applications. The future suggestions of this development technology are listed below;

- Waste heat recovery could be applied at the exhaust of the THS systems in the charging process to increase the energetic and exergetic efficiencies.
- Solar thermal collectors could be used to charge the materials, and then experimental results could be obtained to evaluate economic feasibility of the solar driven THS application.
- Different mixture ratios of inorganic salts of $CaCl_2$-LiCl impregnated into pumice could be developed and investigated to obtain different and better performance results.
- P-$CaCl_2$ and P-$CaCl_2$-LiCl composites could be employed and tested in novel THS reactors for better understanding their performance for real life applications.

REFERENCES

[1] G. Alva, L. Liu, X. Huang, and G. Fang, “Thermal energy storage materials and systems for solar energy applications,” *Renew. Sustain. Energy Rev.*, vol. 68, no. August 2016, pp. 693–706, 2017, doi: 10.1016/j.rser.2016.10.021.

[2] D. Gondre, K. Johannes, and F. Kuznik, “Specification requirements for inter-seasonal heat storage systems in a low energy residential house,” *Energy Convers. Manag.*, vol. 77, pp. 628–636, 2014, doi: 10.1016/j.enconman.2013.09.061.

[3] H. Jarimi *et al.*, “Materials characterization of innovative composite materials for solar-driven thermochemical heat storage (THS) suitable for building application,” *Int. J. Low-Carbon Technol.*, vol. 13, no. 1, pp. 30–42, 2018, doi: 10.1093/ijlct/ctx017.

[4] S. Katuli and M. Cehil, “A novel method for fi nding the optimal heat storage tank capacity for a cogeneration power plant,” vol. 65, pp. 530–538, 2014, doi: 10.1016/j.applthermaleng.2014.01.051.

[5] D. Aydin, S. P. Casey, and S. Riffat, “The latest advancements on thermochemical heat storage systems,” *Renew. Sustain. Energy Rev.*, vol. 41, pp. 356–367, 2015, doi: 10.1016/j.rser.2014.08.054.

[6] G. Krese, R. Koželj, V. Butala, and U. Stritih, “Energy & Buildings Thermochemical seasonal solar energy storage for heating and cooling of buildings,” *Energy Build.*, vol. 164, pp. 239–253, 2018, doi: 10.1016/j.enbuild.2017.12.057.

[7] M. Gaeini, A. L. Rouws, J. W. O. Salari, H. A. Zondag, and C. C. M. Rindt, “Characterization of microencapsulated and impregnated porous host materials based on calcium chloride for thermochemical energy storage,” *Appl. Energy*, vol. 212, no. December 2017, pp. 1165–1177, 2018, doi: 10.1016/j.apenergy.2017.12.131.

[8] M. Karim Nejhad and D. Aydin, “Synthesize and hygro-thermal performance analysis of novel APC-CaCl2 composite sorbent for low-grade heat recovery, storage, and utilization,” *Energy Sources, Part A Recover. Util. Environ. Eff.*, vol. 43, no. 23, pp. 3011–3031, 2021, doi: 10.1080/15567036.2019.1666187.

[9] H. Zhang, T. Yan, N. Yu, Z. H. Li, and Q. W. Pan, “Sorption based long-term thermal energy storage with strontium chloride/ammonia,” *Energy*, vol. 239, 2022, doi: 10.1016/j.energy.2021.122308.

[10] D. Aydin, S. P. Casey, X. Chen, and S. Riffat, “Novel ‘‘ open-sorption pipe ” reactor for solar thermal energy storage,” vol. 121, pp. 321–334, 2016, doi: 10.1016/j.enconman.2016.05.045.

[11] D. Aydin, S. P. Casey, and X. Chen, “Numerical and experimental analysis of a novel heat pump driven sorption storage heater,” vol. 211, no. July 2017, pp. 954–974, 2018, doi: 10.1016/j.apenergy.2017.11.102.

[12] S. P. Casey, D. Aydin, S. Riffat, and J. Elvins, “Salt impregnated desiccant matrices for ‘ open ’ thermochemical energy storage — Hygrothermal cyclic behaviour and energetic analysis by physical experimentation,” *Energy Build.*, vol. 92, pp. 128–139, 2015, doi: 10.1016/j.enbuild.2015.01.048.

[13] H. Zondag, B. Kikkert, S. Smeding, R. De Boer, and M. Bakker, “Prototype thermochemical heat storage with open reactor system,” *Appl. Energy*, vol. 109, pp. 360–365, 2013, doi: 10.1016/j.apenergy.2013.01.082.

[14] L. Shere, S. Trivedi, S. Roberts, A. Sciacovelli, and Y. Ding, “Synthesis and characterization of thermochemical storage material combining porous zeolite and inorganic salts,” pp. 188–191, 2019.

[15] B. Yilmaz, B. Yüksel, G. Orhan, D. Aydin, and Z. Utlu, “Synthesis and characterization of salt-impregnated anodic aluminum oxide composites for low-grade heat storage,” vol. 27, no. 1, pp. 112–118, 2020.

[16] E. Courbon *et al.*, “Further improvement of the synthesis of silica gel and CaCl2 composites: Enhancement of energy storage density and stability over cycles for solar heat storage coupled with space heating applications,” *Sol. Energy*, vol. 157, no. August, pp. 532–541, 2017, doi: 10.1016/j.solener.2017.08.034.

[17] R. van Alebeek, L. Scapino, M. A. J. M. Beving, M. Gaeini, C. C. M. Rindt, and H. A. Zondag, “Investigation of a household-scale open sorption energy storage system based on the zeolite 13X/water reacting pair,” *Appl. Therm. Eng.*, vol. 139, no. March, pp. 325–333, 2018, doi: 10.1016/j.applthermaleng.2018.04.092.

[18] W. G. Haije, J. B. J. Veldhuis, S. F. Smeding, and R. J. H. Grisel, “Solid / vapour sorption heat transformer : Design and performance,” vol. 27, pp. 1371–1376, 2007, doi: 10.1016/j.applthermaleng.2006.10.022.

[19] Z. Xueling *et al.*, “Heat storage performance analysis of ZMS-Porous media/CaCl2/MgSO4 composite thermochemical heat storage materials,” *Sol. Energy Mater. Sol. Cells*, vol. 230, no. July, p. 111246, 2021, doi: 10.1016/j.solmat.2021.111246.

[20] E. Courbon *et al.*, “A new composite sorbent based on SrBr2 and silica gel for solar energy storage application with high energy storage density and stability,” *Appl. Energy*, vol. 190, no. 2017, pp. 1184–1194, 2017, doi: 10.1016/j.apenergy.2017.01.041.

[21] N. Yu, R. Z. Wang, Z. S. Lu, and L. W. Wang, “Development and characterization of silica gel-LiCl composite sorbents for thermal energy storage,” *Chem. Eng. Sci.*, vol. 111, pp. 73–84, 2014, doi: 10.1016/j.ces.2014.02.012.

[22] A. D. Grekova, L. G. Gordeeva, and Y. I. Aristov, “Composite ‘LiCl/vermiculite’ as advanced water sorbent for thermal energy storage,” *Appl. Therm. Eng.*, vol. 124, pp. 1401–1408, 2017, doi: 10.1016/j.applthermaleng.2017.06.122.

[23] P. D’Ans *et al.*, “A new strontium bromide MOF composite with improved performance for solar energy storage application,” *J. Energy Storage*, vol. 25, no. June, p. 100881, 2019, doi: 10.1016/j.est.2019.100881.

[24] S. Z. Xu, R. Z. Wang, L. W. Wang, and J. Zhu, “Performance characterizations and thermodynamic analysis of magnesium sulfate-impregnated zeolite 13X and activated alumina composite sorbents for thermal energy storage,” *Energy*, vol. 167, pp. 889–901, 2019, doi: 10.1016/j.energy.2018.10.200.

[25] E. Piperopoulos, E. Mastronardo, M. Fazio, M. Lanza, S. Galvagno, and C. Milone, “Synthetic strategies for the enhancement of Mg(OH) 2 thermochemical performances as heat storage material,” *Energy Procedia*, vol. 155, pp. 269–279, 2018, doi: 10.1016/j.egypro.2018.11.051.

[26] W. Shi *et al.*, “Water sorption properties of functionalized MIL-101(Cr)-X (X=-NH2, –SO3H, H, –CH3, –F) based composites as thermochemical heat storage materials,” *Microporous Mesoporous Mater.*, vol. 285, no. April, pp. 129–136, 2019, doi: 10.1016/j.micromeso.2019.05.003.

[27] E. Courbon, P. D’Ans, O. Skrylnyk, and M. Frère, “New prominent lithium bromide-based composites for thermal energy storage,” *J. Energy Storage*, vol. 32, no. July, p. 101699, 2020, doi: 10.1016/j.est.2020.101699.

[28] Y. N. Zhang, R. Z. Wang, and T. X. Li, “Experimental investigation on an open sorption thermal storage system for space heating,” *Energy*, vol. 141, pp. 2421–2433, 2017, doi: 10.1016/j.energy.2017.12.003.

[29] A. H. Abedin and M. A. Rosen, “Closed and open thermochemical energy storage : Energy- and exergy-based comparisons,” *Energy*, vol. 41, no. 1, pp. 83–92, 2012, doi: 10.1016/j.energy.2011.06.034.

[30] M. S. Buker, B. Mempouo, and S. B. Riffat, “Performance evaluation and techno-economic analysis of a novel building integrated PV/T roof collector: An experimental validation,” *Energy Build.*, vol. 76, pp. 164–175, 2014, doi: 10.1016/j.enbuild.2014.02.078.